Solid Earth

Tectonic processes, variations in sediment flux, and eustatic sea level recorded by the 20 Myr old Burdigalian transgression in the Swiss Molasse basin

Philippos Garefalakis and Fritz Schlunegger

Institute of Geological Sciences, University of Bern, Bern, 3012, Switzerland

Correspondence: Philippos Garefalakis (philippos.garefalakis@geo.unibe.ch)

Abstract. The stratigraphic architecture of the Swiss Molasse basin, situated on the northern side of the evolving Alps, reveals crucial information about the basin's geometry, its evolution, and the processes leading to the deposition of the siliciclastic sediments. Nevertheless, the formation of the Upper Marine Molasse (OMM) and the controls on the related Burdigalian transgression have still been a matter of scientific debate. During the time period from ca. 20 to 17 Ma, the Swiss Molasse basin was partly flooded by a shallow marine sea striking SW–NE. Previous studies have proposed that the transgression occurred in response to a rise in global sea level, a reduction of sediment flux, or an increase in tectonically controlled accommodation space. Here, we readdress this problem and extract stratigraphic signals from the Burdigalian molasse deposits that can be related to changes in sediment supply rate, variations in the eustatic sea level, and subduction tectonics. To achieve this goal, we conducted sedimentological and stratigraphic analyses of several sites across the entire Swiss Molasse basin.

Field investigations show that the transgression and the subsequent evolution of the Burdigalian seaway was characterized by (i) a deepening and widening of the basin, (ii) phases of erosion and non-deposition during Lower Freshwater Molasse (USM), OMM, and Upper Freshwater Molasse (OSM) times, and (iii) changes in along-strike drainage reversals. We use these changes in the stratigraphic record to disentangle tectonic and surface controls on the facies evolution at various scales. As the most important mechanism, rollback subduction of the European mantle lithosphere most likely caused a further downwarping of the foreland plate, which we use to explain the deepening and widening of the Molasse basin, particularly at distal sites. In addition, subduction tectonics also caused the uplift of the Aar massif. This process was likely to have shifted the patterns of surface loads, thereby resulting in a buckling of the foreland plate and influencing the water depths in the basin. We use this mechanism to explain the establishment of distinct depositional settings, particularly the formation of subtidal shoals wherein a bulge in relation to this buckling is expected. The rise of the Aar massif also resulted in a reorganization of the drainage network in the Alpine hinterland, with the consequence that the sediment flux to the basin decreased. We consider this reduction in sediment supply to have amplified the tectonically controlled widening and deepening of the Molasse basin. Because the marine conditions were generally very shallow, subtle changes in eustatic sea level contributed to the formation of several hiatuses that chronicle periods of erosion and non-sedimentation. These processes also amplified the tectonically induced increase in accommodation space during times of global sea level highstands. Whereas these mechanisms are capable of explaining the establishment of the Burdigalian seaway and the formation of distinct sedimentological niches in the Swiss Molasse basin, the drainage reversal during OMM times possibly requires a change in tectonic processes at the slab scale, possibly including the entire Alpine range between the Eastern and Central Alps.

In conclusion, we consider rollback tectonics to be the main driving force controlling the transgression of the OMM in Switzerland, with contributions by the uplift of individual crustal blocks (here the Aar massif). In addition, the reduction of sediment flux was likely to have been controlled by tectonic processes as well when basement blocks became uplifted, thereby modifying the catchment geometries. Eustatic

Please note the remarks at the end of the manuscript.

changes in sea level explain the various hiatuses and amplified the deepening of the basin during eustatic highstand conditions.

1 Introduction

Foreland basins and their deposits have often been used to explore the tectonic evolution of their hinterlands, mainly because these basins are mechanically coupled with the adjacent mountain belts (Beaumont, 1981; Jordan, 1981; DeCelles, 2004). The formation of these foreland basins occurs through the flexural downwarping of the underlying lithosphere in response to loading, which results in the formation of a wedge-shaped trough where sediment accumulates (DeCelles and Giles, 1996; Allen and Allen, 2005). The shape of the foreland trough depends on the mechanical properties of the foreland plate (Sinclair et al., 1991; Flemings and Jordan, 1990; Jordan and Flemings, 1991), the load of the sedimentary fill itself (Flemings and Jordan, 1990; Jordan and Flemings, 1991), and predominantly the tectonic and geodynamic processes leading to changes in plate loading (Beaumont, 1981; Jordan, 1981; Allen et al., 1991; Sinclair et al., 1991; DeCelles and Gilles, 1996). Additionally, a foreland basin can either be occupied by a peripheral sea when sediment flux is lower than the formation rate of accommodation space or by a fluvial system if the opposite is the case (Sinclair and Allen, 1992). A shift from terrestrial to marine conditions, for instance, can occur through a reduction in sediment flux, an increase in tectonically controlled subsidence rate (Sinclair et al., 1991), or a rise in the eustatic sea level (Reichenbacher et al., 2013). This has particularly been inferred for the North Alpine Foreland Basin, or the Molasse basin, situated on the northern side of the European Alps (Fig. 1a), which experienced a change from terrestrial to marine conditions during Burdigalian times ca. 20 Myr ago (e.g. Matter et al., 1980; Pfiffner, 1986; Schlunegger et al., 1997a; Kempf et al., 1999; Kuhlemann and Kempf, 2002; Ortner et al., 2011). In the Swiss part, this transgression resulted in the establishment of a shallow marine seaway, linking the Paratethys in the NE with the Tethys in the SW (Allen et al., 1985), and it is recorded by the deposition of the Upper Marine Molasse group (OMM; Matter et al., 1980; P. A. Allen, 1984). Although the history and geometry of the Burdigalian seaway and the related sedimentary processes are well known through detailed sedimentological and chronological investigations (e.g. Lemcke et al., 1953; P. A. Allen TS1, 1984; Allen et al., 1985; Homewood et al., 1986; Doppler, 1989; Keller, 1989; Jin et al., 1995; Salvermoser, 1999; Strunck and Matter, 2002; Kuhlemann and Kempf, 2002; Reichenbacher et al., 2013), the controls on this transgression have still been a matter of ongoing scientific debate. Previous authors (e.g. Allen et al., 1985; Homewood et al., 1986; Keller, 1989; Strunck and Matter,

2002; Reichenbacher et al., 2013) proposed a combination of a reduced sediment flux and a rise in global sea level as possible mechanisms. However, thermo-chronometric data from the core of the Alps (Lepontine dome, Fig. 1; Boston et al., 2017) and structural work in the external Aar massif (Fig. 1; Herwegh et al., 2017) revealed that the Burdigalian was also the time of major tectonic events, including thrusting in the Aar massif and tectonic exhumation of the Lepontine dome (Schmid et al., 1996), leading to changes in surface loads in the Alps. Accordingly, it was proposed that tectonic processes could also have controlled the transgression of the peripheral sea through downwarping of the foreland plate (Sinclair et al., 1991). It is possible that the Swiss part of the Molasse basin bears key information to differentiate between these underlying mechanisms (eustasy, sediment flux, tectonics) because it is situated to the north of the Aar massif and the Lepontine dome (Fig. 1).

The aim of this paper is to disentangle tectonic processes, a reduction of sediment flux, and changes in the eustatic sea level as controls on the transgression of the OMM in the Swiss Molasse. We analysed OMM outcrops and sections along the entire Swiss Molasse basin at both proximal and distal positions relative to the Alpine front (Fig. 1a). To this extent, we measured palaeo-flow directions, and we explored the OMM deposits for their sedimentary facies and related depositional settings. We also determined the thickness and grain size of sedimentary bedforms, and we applied hydrological concepts to calculate palaeo-water depths based on the measured parameters. However, a chronological framework is absolutely required for correlating sections across a basin where facies relationships are strongly heterochronous, as is the case for the Swiss Molasse basin (Matter et al., 1980). Therefore, we also reassessed the temporal framework of the analysed sections through a compilation of previously published magnetostratigraphic and biostratigraphic data, and we correlated the individual sections across the basin.

2 Geological setting

2.1 The architecture and evolution of the Alps

The doubly vergent Alpine orogen (Fig. 1) is the consequence of the late Cretaceous to present continent–continent collision between the European and Adriatic plates (Schmid et al., 1996; Handy et al., 2010). It is comprised of a double vergent nappe stack wherein the material on the northern side was derived from the European and Adriatic plates, while the rocks on the southern side is only of Adriatic provenance. In the centre, the Alps expose a crystalline core of European origin referred to as the Lepontine dome and the external massifs (Fig. 1; e.g. Aar massif; Spicher, 1980). At deeper crustal levels, the Alpine orogen is underlain by a thick crustal root made up of a stack of lower crustal material derived from the
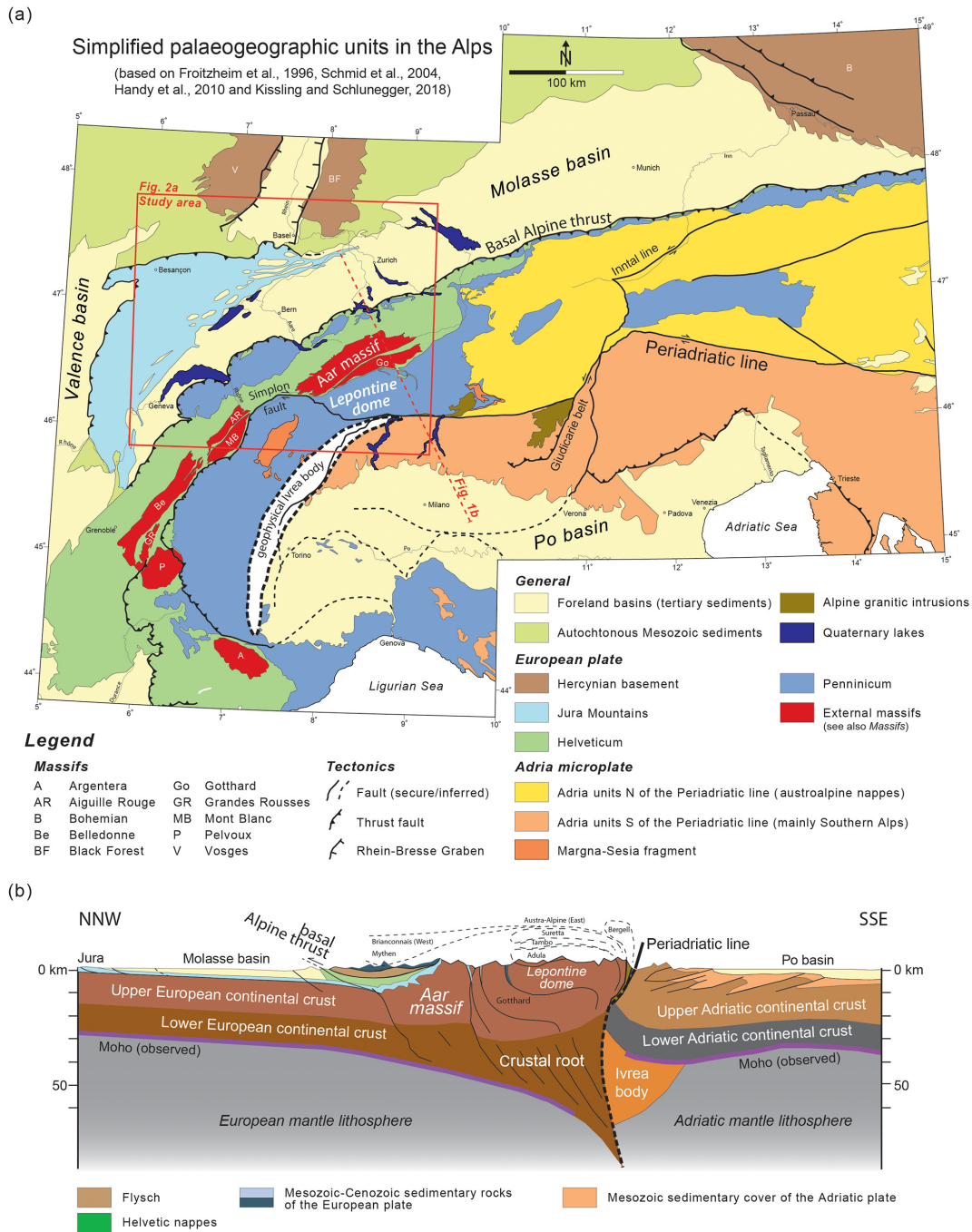
Figure 1. (a) Simplified geological map of the European Alps based on a compilation by Kissling and Schlunegger (2018) and updated using additional information from Handy et al. (2015) and Pippèrr and Reichenbacher (2017); note the location of Fig. 2a and trace of **(b)**. **(b)** Simplified geological–geophysical section through the Central European Alps adapted from Kissling and Schlunegger (2018).

European continental plate (Fry et al., 2010; Fig. 1b). Beneath the core of the orogen, the ca. 160 km long (Lippitsch et al., 2003) lithospheric mantle slab of the European continental plate bends and thus downwarps the foreland plate towards the SE (Fig. 1b). This bending was mainly driven by slab load due to the relatively large density of the subducted lithospheric mantle in comparison with the surrounding asthenosphere as seismo-tomography data reveal (Lippitsch et al., 2003). On the northern side of the Alps, the structurally highest unit is made up of Austroalpine nappes that structurally overlie the Penninicum, which in turn are underlain by the Helvetic thrust nappes (Fig. 1a). The front of the Hel-

vetic and Penninicum units is referred to as the basal Alpine thrust (Fig. 1b). On the southern side, the Alps are made up of the south alpine thrust sheets that consist of crystalline basement rocks and sedimentary units of African origin. This fold-and-thrust belt is bordered to the south by the Po basin (Fig. 1a). The northern side of the Alps are separated from the southern side by the north-dipping Periadriatic line that accommodated most of the shortening during the Oligocene and the early Miocene by backthrusting and right-lateral slip (Schmid et al., 1996).

Recently, slab load has been considered the major driving force of the subduction history of the European plate and for the exhumation of crystalline rocks (Kissling and Schlunegger, 2018). This also concerns the exhumation of the Lepontine dome (Fig. 1), where normal faulting along the Simplon detachment fault resulted in rapid tectonic exhumation of the dome between late Oligocene and early Miocene times with a peak recorded by thermo-chronometric data at 20 Ma (Fig. 1b; Hurford, 1986; Mancktelow, 1985; Mancktelow and Grasemann, 1997; Schlunegger and Willett, 1999; Boston et al., 2017). This was also the time when the Aar massif, situated on the European continental plate (Fig. 1b), experienced a period of rapid vertical extrusion (Herwegh et al., 2017). Herwegh et al. (2017) and Kissling and Schlunegger (2018) proposed a mechanism referred to as rollback subduction to explain these observations. According to these authors, delamination of crustal material from the European mantle lithosphere along the Moho resulted in a stacking of buoyant lower crustal rocks beneath the Lepontine dome and the Aar massif, forming the crustal root (Fry et al., 2010; Fig. 1b). These processes are considered to have maintained isostatic equilibrium between the subducted lithospheric mantle and the crust and thus the elevated topography (Schlunegger and Kissling, 2015). Additionally, they most likely balanced, through the stacking of the crustal root (Fry et al., 2010, Fig. 1b), the rapid removal of upper crustal material in the Lepontine dome at ca. 20 Ma (Schlunegger and Willet, 1999; Boston et al., 2017). Delamination of crustal material has also been invoked to explain the contemporaneous rapid exhumation and northward thrusting of the Aar massif along steeply dipping thrusts (Herwegh et al., 2017). These processes were contemporaneous with (i) the reorganization of the drainage network of the Central Alps (Kuhlemann et al., 2001a; Schlunegger et al., 1998), (ii) the decrease in sediment flux to the basin, as revealed by sediment budgets (Kuhlemann, 2000; Kuhlemann et al., 2001a, b), and (iii) the Burdigalian transgression in the Swiss part of the Molasse basin. We will thus refer to these processes when discussing the controls on the Burdigalian transgression within a geodynamic framework.

2.2 The architecture and evolution of the Molasse basin

The Molasse basin is approximately 700 km long and striking ENE–WSW from France to Austria, where it broadens from < 30 km to a maximum width of ca. 150 km (Pfiffner, 1986; Fig. 1a). It is limited to the north by the Jura Mountains, the Black Forest, and Bohemian massifs, as well as to the south by the basal Alpine thrust (Homewood et al., 1986).

Reconstructions of the evolution of the Molasse basin (Fig. 2a) have been the focus of many research articles over the past years (e.g. Matter et al., 1980; Homewood and Allen, 1981; P. A. Allen, 1984; Keller, 1989; Schlunegger et al., 1996; Sinclair, 1997; Kempf et al., 1999; Kuhlemann and Kempf, 2002; Ortner et al., 2011; Reichenbacher et al., 2013). This has resulted in the general notion that the large-scale subsidence history of the Molasse basin was closely linked with the geodynamic evolution of the Alps (Sinclair et al., 1991; Kuhlemann and Kempf, 2002; Pfiffner et al., 2002; Ortner et al., 2011; Schlunegger and Kissling, 2015). The development of this basin as a foreland through has been considered to commence with the closure of the Alpine Tethys in late Cretaceous times (Lihou and Allen, 1996; Schmid et al., 1996). This was the time when subduction of the European oceanic lithosphere with a large density beneath the Adriatic continental plate started. Large slab load forces resulted in a downwarping of the European foreland plate and the formation of a deep marine trough (Schmid et al., 1996), where sedimentation occurred by turbidites (Sinclair, 1997) on submarine fans (Allen et al., 1991; Sinclair, 1997; Lu et al., 2018; Reichenwallner, 2019). This first period of basin evolution has been referred to as the flysch stage in the literature (Fig. 2b; Sinclair and Allen, 1992). The situation changed at 35–32 Ma when the buoyant continental lithosphere of the European plate started to enter the subduction channel. Strong tension forces started to operate at the stretched margin of the European continental crust, particularly beneath the Central Alps (Schmid et al., 1996), with the result that the subducted oceanic lithosphere of the European plate broke off (Davies and von Blanckenburg, 1995). The consequence was a rebound of the European plate, a rise of the Central Swiss Alps, and an increase in sediment flux to the Swiss Molasse basin (Sinclair, 1997; Kuhlemann et al., 2001a, b; Willett, 2010; Garefalakis and Schlunegger, 2018), which became overfilled at ca. 30 Ma (Sinclair and Allen, 1992; Sinclair, 1997). The subsequent post-30 Ma stage of basin evolution has been referred to as the molasse stage (Sinclair and Allen, 1992).

Molasse sedimentation occurred from ca. 30 Ma onward and was recorded by two large-scale, transgressive–regressive mega-sequences (Fig. 2b; e.g. Sinclair, 1997; Kempf et al., 1997, 1999; Kuhlemann and Kempf, 2002; Cederbom et al., 2004, 2011). These two mega-sequences consist of four lithostratigraphic groups. The first mega-sequence comprises the Lower Marine Molasse (UMM; Diem, 1986) and the Lower Freshwater Molasse (USM; Platt and Keller, 1992), and the second mega-sequence consists of the Upper Marine Molasse (OMM; Homewood et al., 1986) and the Upper Freshwater Molasse (OSM; Matter et al., 1980). Sedimentation in the Molasse basin continued up
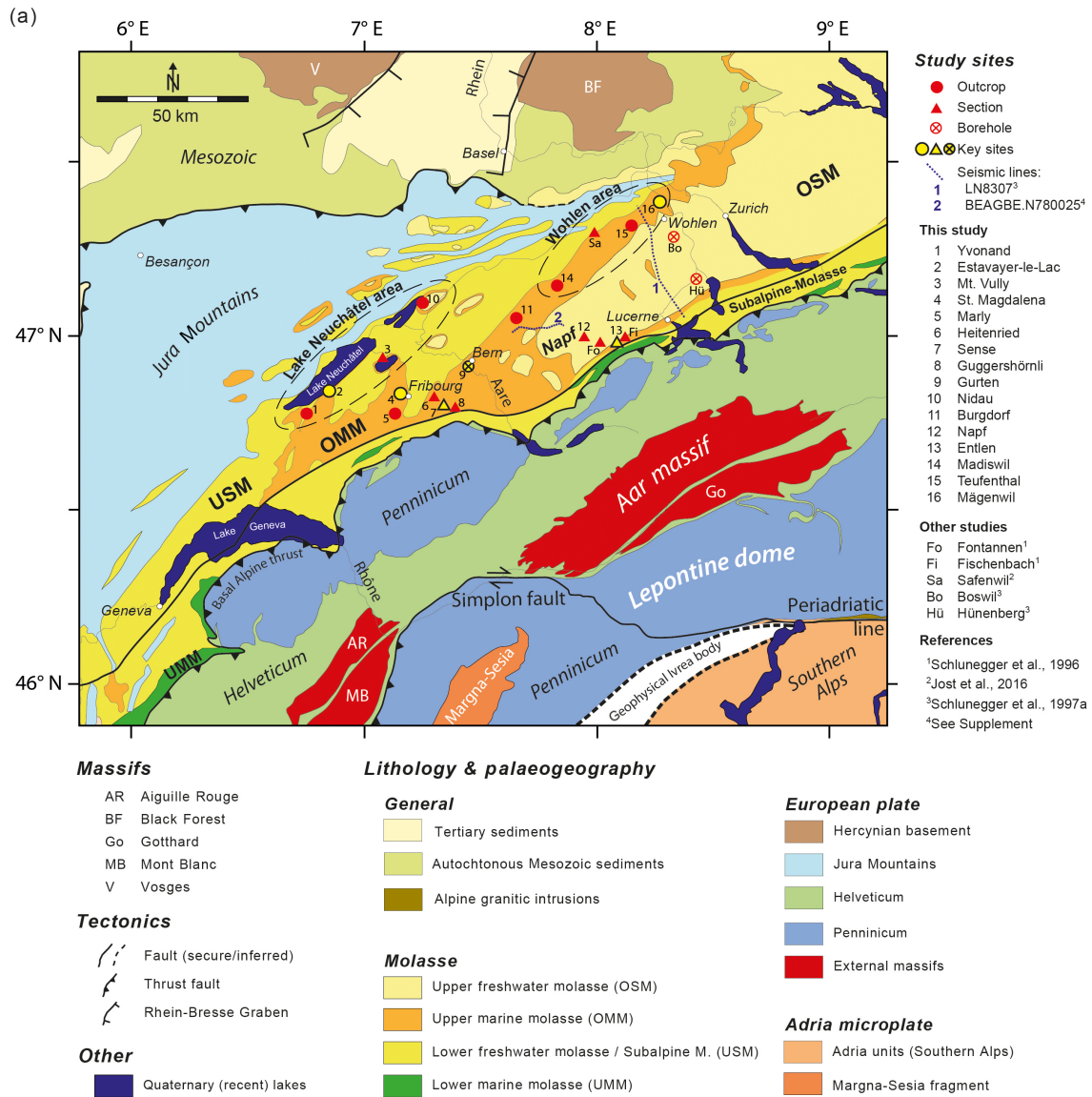
(a)

Figure 2.

to ca. 10–5 Ma, when a phase of uplift during Pliocene times resulted in erosion and recycling of the previously deposited Molasse units (Mazurek et al., 2006; Cederbom et al., 2004, 2011). This erosion reached deeper stratigraphic levels in the western part of the Molasse basin than in the eastern segment (Baran et al., 2014) with the consequence that the OMM deposits are only fragmentarily preserved in the west (Fig. 2a).

Sediment dispersal changed during the molasse stage of basin evolution. Prior to 20 Ma, during USM times, measurements of sediment transport directions (Kempf, 1998; Kempf et al., 1999) and sediment provenance analysis (Füchtbauer, 1964) revealed that the sedimentary material was transported to the east by braided to meandering streams. At that time, a

coastline was situated near Munich, separating a deep marine trough farther east from a terrestrial environment to the west of Munich (Kuhlemann and Kempf, 2002). During OMM times, heavy mineral assemblages reveal that the Swiss Molasse basin operated as a closed sedimentary trough, where all supplied material was locally stored (Allen et al., 1985). During OSM times, from ca. 16.5 to 5 Ma, heavy mineral data imply that material with sources in the Hercynian basement north of Munich or the Bohemian massif was supplied to the Swiss Molasse ("Graupensandrinne"; Allen et al., 1985; Berger, 1996), suggesting that material transport occurred towards the west (Kuhlemann and Kempf, 2002). The details of the reversal of the drainage direction have not yet
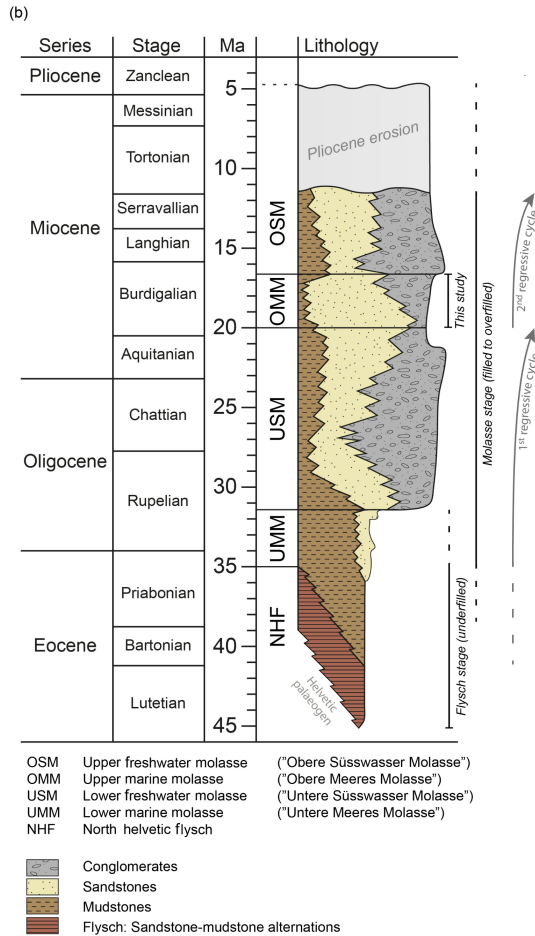
Figure 2. (a) Detailed geological map of the area between Geneva and Zurich adapted from Kissling and Schlunegger (2018) showing the locations of data points referred to in this paper. The OMM deposits at sites 1 to 16 have been mapped at the scale of 1 : 25 000, which was used to reproduce Fig. 6. In addition, the observations of the sections, outcrops, and drill core at sites 2, 4, 7, 9, 12, 13, and 16 are explicitly described in Sects. 4 and 5 of this paper. Please refer to Fig. 1 for the complete legend. **(b)** Lithostratigraphic scheme of the Molasse deposits in Switzerland. Modified after Keller (1989).

been elaborated, and related scenarios lack a database with palaeo-flow information, particularly for the OMM. The establishment of such a database, particularly the assignment of a more precise age to the drainage reversal, will be part of the scope of this article.

2.3 The Upper Marine Molasse

2.3.1 Lithostratigraphic and sedimentological framework

The Upper Marine Molasse (OMM) deposits, which are the focus of this study, mainly consist of a suite of shallow marine sandstones and mudstones that were deposited between ca. 20 and 17 Ma (Fig. 2b) in a ca. 70–80 km wide sea-

way (Allen and Homewood, 1984; Allen et al., 1985; Keller, 1989; Strunck and Matter, 2002). Close to the Alpine thrust front, the OMM successions are up to 900 m thick and thin to a few tens of metres towards the distal basin margin farther northwest.

Large streams with sources in the Central Alps supplied their material to the Molasse basin, thereby forming megafans and conglomerate deposits with diameters > 10 km that interfingered with the sea (Schlunegger et al., 1996; Kempf et al., 1999). Consequently, the facies relationships were strongly heterochronous across the basin, and terrestrial deposits, preserved as conglomerates of the OSM according to Matter (1964), grade into marine sediments of the OMM (Keller, 1989) over a lateral distance of a few tens of kilometres. This is also the case in the study area, where thick conglomerate packages situated at the Alpine thrust front ca. 50 km to the NE of the Aar massif (Napf conglomerates; Matter, 1964; Haldemann et al., 1980) separate the basin into southeastern and northwestern segments with different lithostratigraphic schemes (Fig. 3a). For simplicity purposes, these areas will be referred to as the eastern and western segments in relation to the Napf. East of the Napf conglomerates, in the following text denoted as the Napf units (Matter, 1964), the OMM has been grouped in two transgressive–regressive packages referred to as the Lucerne and the St. Gallen formations (Keller, 1989). Both units comprise a suite of sandstones with mudstone interbeds. They are separated from each other by a metre-thick palaeosol (Schlunegger et al., 2016). We will refer to these units as the OMM-I (Lucerne Fm) and the OMM-II (St. Gallen Fm), respectively (Fig. 3a). Keller (1989) additionally categorized the OMM-I east of the Napf units into a lower wave-dominated unit and an upper unit where tidal processes are recorded, which we refer to as the OMM-Ia and OMM-Ib, respectively.

West of the Napf, the OMM at the proximal basin border has also been categorized in two units (Fig. 3a) but with a different scheme and different names. These are the Sense Formation at the base (suite of sandstones with mudstone interbeds) and the Kalchstätten Formation at the top (alternation of sandstones and mudstones). Further up-section, these marine deposits (Strunck and Matter, 2002) grade into the fluvial conglomerates of the Guggershorn Formation and thus into the OSM (Strunck and Matter, 2002) (Fig. 3a). Magnetostratigraphic dating showed that the accumulation of the Guggershorn Formation occurred contemporaneously with marine (OMM) sedimentation at more distal sites. These conglomerates thus represent the deposits of a braided stream that shed its material to the OMM sea, similar to the Napf conglomerates.

In the central basin near Fribourg (Fig. 2a), also on the western side of the Napf, sedimentological investigations of sand waves (Homewood and Allen, 1981; Homewood et al., 1986) disclosed the occurrence of tidal bundles and a bidirectional dispersal of sedimentary material. These deposits

(a)
Lithostratigraphic scheme to the west of the napf

Lithostratigraphic scheme at the napf

Lithostratigraphic scheme to the east of the napf

Lithostratigraphic scheme of sections in the distal basin
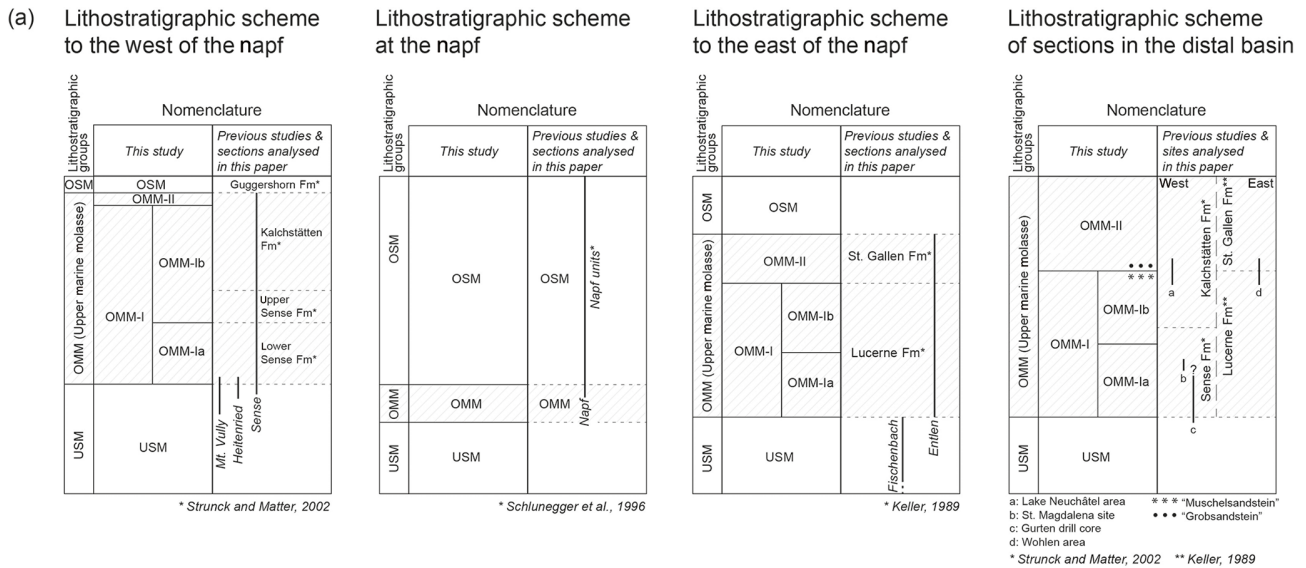
Figure 3.

have been assigned to a subtidal environment (Homewood and Allen, 1981) where material with sources in the Central Alps was redistributed in the basin by strong tidal currents that entered the basin from the Tethys in the south and the Paratethys in the northeast (Allen et al., 1985; Kuhlemann and Kempf, 2002; Bieg et al., 2008). Lithostratigraphic correlations suggest that the deposits at Fribourg most likely correspond to the lower Sense Fm (Python, 1996) and thus to the OMM-Ia (see the Discussion section and Fig. 3a).

In the basin axis, between the Lake Neuchâtel and Wohlen areas (Fig. 2a), coarse-grained sandstones with large-scale cross-beds in which individual grains are larger than 2 mm have been interpreted as subtidal sand waves (Allen and Homewood, 1984; Allen et al., 1985). These deposits are calcareous sandstones with shelly fragments, referred to as the "Muschelsandstein" (Allen and Homewood, 1984; Allen et al., 1985, Fig. 3a). Alternatively, they occur as coarse-grained cross-bedded sandstones with large lithoclasts, also called the "Grobsandstein" (Jost et al., 2016).

2.3.2 Chronostratigraphic framework

Ages for the OMM deposits have been established by multiple authors through palaeontological analyses of mammalian fragments and teeth (Keller, 1989; Schlunegger et al., 1996; Kempf et al., 1999) as well as $^{87}Sr/^{86}Sr$ chemostratigraphy (Keller, 1989). The latter yield a numerical age between ca. 18.5 and 17 Ma, particularly for the OMM-II on the eastern side of the Napf. Subsequent magneto-polarity chronologies (Schlunegger et al., 1996; Strunck and Matter, 2002) paired with further micro-mammalian discoveries (Kempf et al., 1997; Kempf, 1998; Kälin and Kempf, 2009; Jost et al., 2016) allowed for an update of the chronological framework (Fig. 3b) of Keller (1989) through correla-

tions with the magneto-polarity timescale (MPTS) of Cande and Kent (1992, 1995) and the most recent astronomically tuned Neogene timescale (ATNTS; Lourens et al., 2004). This yielded the notion that the transgression of the peripheral sea and the deposition of the OMM started at ca. 20 Ma and was synchronous, within uncertainties, across the entire Swiss Molasse basin (Strunck and Matter, 2002). However, a temporal correlation of sections across the Napf, i.e. between eastern and western Switzerland (Fig. 3a), and a harmonization of the stratigraphic schemes (Fig. 3b) have not been achieved yet. This will be accomplished in this paper, and it will build the temporal framework for the discussion of the development of the basin.

3 Methods

3.1 Location of sections and available database

Following the scope of the paper, we established the facies relationships and sediment transport patterns during the transgressive phase of the OMM and thus mainly focused on the OMM-I. We proceeded through sedimentological investigations of key sites (Fig. 2a), which expose the related succession in proximal (Entlen section east of the Napf units; Sense section west of the Napf units), central (St. Magdalena site, Gurten drill core), and distal positions (Lake Neuchâtel and Wohlen areas). The lithofacies in the Entlen and Sense sections was investigated in the field at the scale of 1 : 50. At each outcrop along these sections, data were collected as notes in the field book and hand drawings on digital photos (available from the senior author upon request). The results are then presented as logs in Fig. 4 and in Tables 1 and 2. The St. Magdalena site and the Lake Neuchâtel and Wohlen
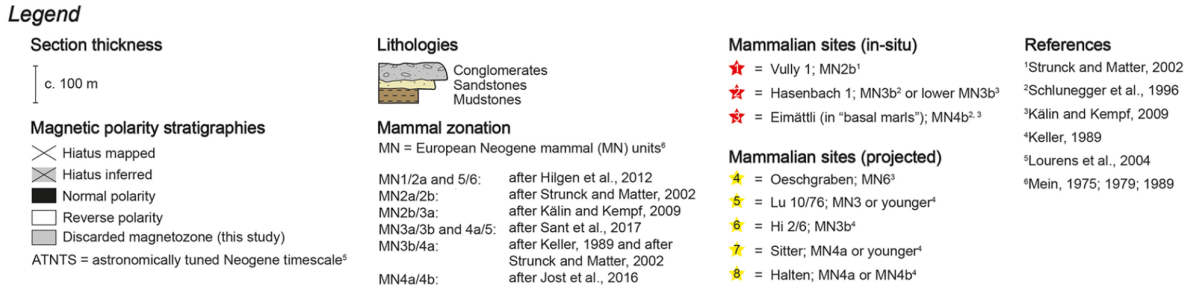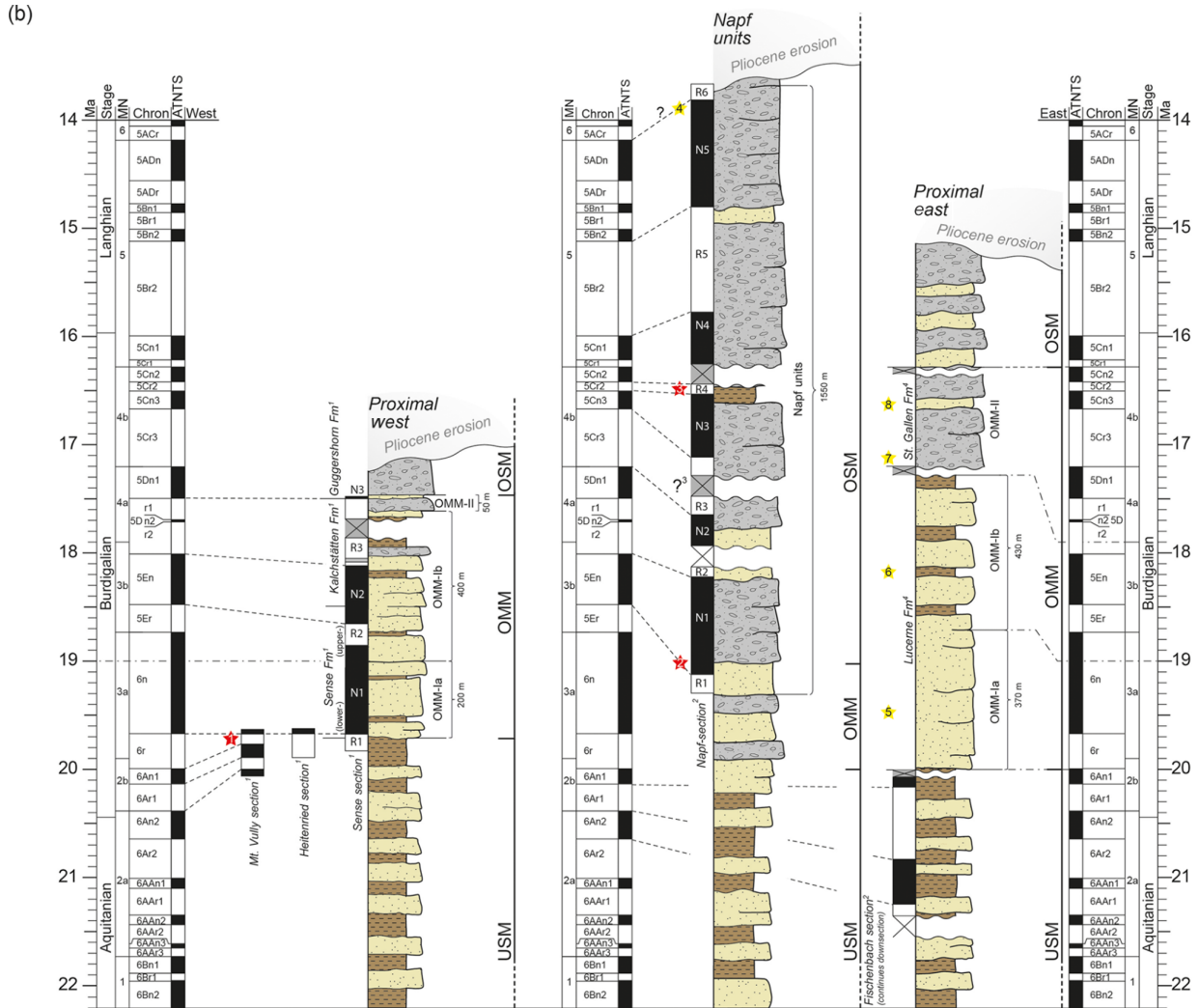
Figure 3. (a) Lithostratigraphic scheme of the OMM in Switzerland. **(b)** Composite stratigraphic columns illustrating sedimentary architectures at the proximal basin border in the western Molasse basin (proximal west), in the central part of the Molasse basin (Napf units), and in the eastern basin (proximal east). The composite section for the proximal western basin is based on data from the Mt. Vully and Heitenried sections, drillings, and from surface information from the Sense section (Sense beds and Kalchstätten Formation) (Strunck and Matter, 2002). The composite section representative of the central part of the Molasse basin (Napf) is mainly based on the sedimentary logs by Schlunegger et al. (1996; see their Schwändigraben and Fontannen sections) complemented with information from the geological map of the region (Schlunegger et al., 2016). Note that Kälin and Kempf (2009) proposed a very short hiatus recorded by magnetozone R3 within the Napf units, which we do not discuss in detail for simplicity purposes. The composite section illustrating the situation at the proximal basin border east of the Napf represents the sedimentary architecture as far east as Lake Zurich (Fig. 2a). It is based on data from Keller (1989, see his Rümlig, Ränggloch, and Lucerne sections) and from Schlunegger et al. (1996, see their Fischenbach section) and geological maps of the region (Wolhusen; Isler and Murer, 2019). Note that the Entlen section is situated immediately east of the Napf (Fig. 5a) where the lowermost part (Lucerne Formation) can be characterized by the composite section of the proximal east. Detailed sedimentological data of the Sense Formation and the Lucerne Formation are shown in Fig. 4. Note that the Molasse units shown in capitals (i.e. USM, OMM, and OSM) are based on the lithological architecture and thus on facies associations identified in the field.

areas only display outcrops rather than sections. Therefore, the sediments at these locations have been sketched in the field and on digital photos, thereby paying special attention to collecting information about the orientation and thickness of cross-beds. The sedimentary material of the ca. 200 m deep Gurten drill core is not available. However, the sediments were photographed at high resolution at the University of Bern in 1989 (see Fig. S3 in the Supplement). We used these photos to extract information on the lithofacies association encountered in the drilling.

3.2 Reconstruction of sedimentary architecture

The lithofacies have been identified (e.g. Schaad et al., 1992; Keller, 1989) based on the assemblage of sedimentary characteristics, including grain size, thickness, lateral extent if applicable, sedimentary structures, basal contact, colour, and fossil content (Tables 1 to 5). The lithofacies types correspond to individual bedforms (see Tables 1 to 5 for references), which bear information on flow strengths, flow directions, sediment supply, and water depths (e.g. Keller, 1989). The combination of these parameters, usually recorded by distinct assemblages of lithofacies types, can be used to identify distinct sedimentary settings. Related concepts of facies analysis have been documented for fluvial deposits (Miall, 1978, 1985, 1996; Platt and Keller, 1992) but are less standardized for shallow marine deposits. Here, we followed Keller (1989) and Schaad et al. (1992), who developed a concept for shallow marine deposits whereby lithofacies types are grouped into facies assemblages in a hierarchic order, based on which distinct shallow marine settings can be interpreted. We followed these authors and assembled the various lithofacies types into five depositional settings, which are from land to sea: terrestrial, backshore, foreshore, nearshore, and offshore. We then mapped the depositional settings at the scale of 1 : 25 000 at various sites across the Swiss Molasse basin where suitable outcrops were present (see Fig. 2a for visited sites).

3.3 Determination of sediment transport directions

Sediment transport directions were determined from orientations of clast imbrications, gutter casts, and dip directions of cross-beds. In addition, the orientation of the coastline can be inferred from sediment transport within the surf- and-swash zone at the wet beach where rolling grains carve millimetre-thin rills in the beach deposits, which are oriented perpendicular to the coast. These rills are recorded by linear grooves, or parting lineations, on the surface of sandstones (J. R. L. Allen, 1982; Hammer, 1984). We thus measured the orientation of these features where visible. We also determined the strike direction of oscillation ripple marks to infer the orientation of waves and thus of the coastline.

3.4 Calculation of palaeo-water depths

We analysed the sediments in the key sections according to their palaeo-water depths. For oscillation ripple marks, the ripple metrics (spacing between ripple crests and ripple heights) together with the grain size can be used to infer water depths at the time the oscillation ripples were formed (Diem, 1985; Allen et al., 1985; the Supplement). We thus measured the ripple metrics with a metre stick together with grain sizes in the field and calculated the water depths following Allen (1997). Likewise, minimum water depths can be inferred from the heights of cross-beds as examples from modern streams have shown (Bridge and Tye, 2000; Leclair and Bridge, 2001). Please refer to the Supplement for the deviation of the related equations. Published information from deep drillings (Boswil 1; Hünenberg 1; Schlunegger et al., 1997a) and seismostratigraphic data (line 8307, Schlunegger et al., 1997a; line BEAGBE.N780025; Fig. S2 in the Supplement) completed the available database.

4 Results

4.1 Proximal basin border to the east of the Napf: Entlen section (site 13 in Fig. 2a)

The sedimentary suite of the ca. 370 metre thick OMM-Ia at Entlen (Figs. 4a and S4a in the Supplement) records a large diversity of lithofacies types (Table 1). Parallel-laminated (Sp), fine- to medium-grained sandstone packages are centimetres to decimetres thick and normally graded. These deposits alternate with decimetre-thick low-angle cross-bedded units with tangential lower boundaries (Sc, Sct_a) and layers with a massive structure (Sm). Gravel and pebble layers (Sg) and shell fragments (Shf) are visible where sandstone units have erosive bases. Current (Scr) and oscillation ripple marks (Sos), locally with branching crests (Sbr), as well as flame fabrics or sand volcanoes (Sv) are present only in some places. Fine-grained lithofacies include millimetre- to centimetre-thick parallel-laminated to massive mudstone layers (Mp, Mm). Siltstone climbing ripples (Mcl) are subordinate in the OMM-Ia suite. Mudstone drapes (Md), a few millimetres thick, mostly occur on top of current ripple marks (Scr). In places, root casts are associated with yellow to ochre mottled colours.

The overlying ca. 430 m thick OMM-Ib (Figs. 4a and S4a in the Supplement) comprises fine- to medium-grained sandstone packages with mudstone interbeds (Table 1). Low-angle trough (Sct_r) or tabular (Sct_a) cross-bedded sandstone beds are several decimetres thick. The Sct_r sandstones contain current ripple marks (Scr) at their base, whereas laminae sets of Sct_a sandstones are interbedded with current ripples (Scr) recording an opposing sediment transport direction. At one site, decimetre-thick sandstone beds display a planar base and a wavy top with a wavelength of several
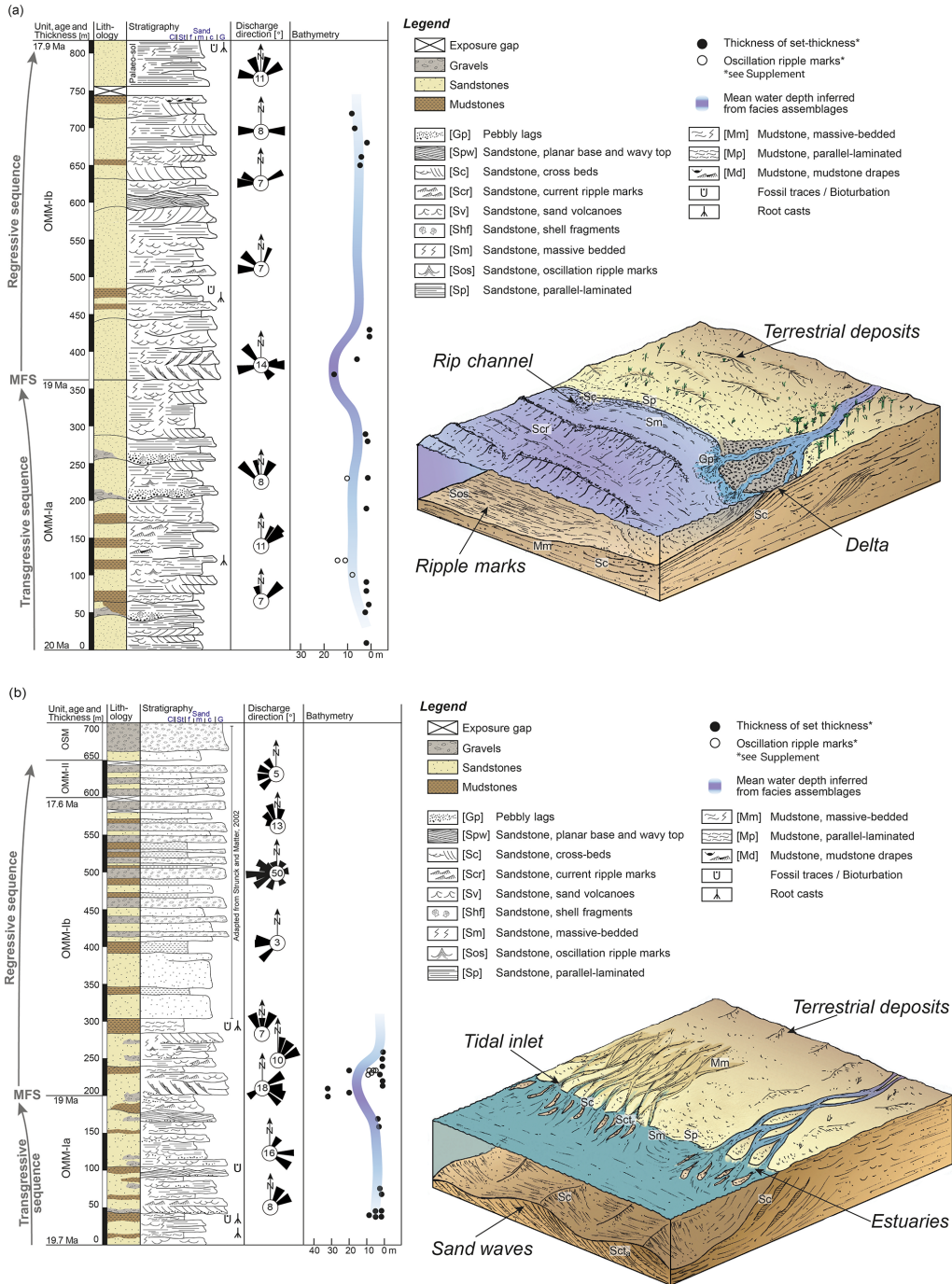
Figure 4. Sedimentological logs of **(a)** the Entlen and **(b)** the Sense section. See Fig. 2a for the locations of sections, Fig. 5 for the chronological framework of the deposits, and the tables for further sedimentological details, abbreviations of the lithofacies, and references to sedimentological work. The block diagrams illustrate the palaeogeographical conditions from a conceptual point of view. Note that the palaeo-bathymetric values are minimum estimates and that the mean water depths have been inferred from the assignment of lithofacies to a depositional setting. This might explain why the numerical values for water depths based on cross-bed thicknesses and our inferred mean water depth estimates deviate between ca. 200 and 250 m of the Sense section.

Table 1. Lithofacies encountered in the Entlen section.

Facies assemblages	Structures and bedforms	Depositional setting and references
Mcl, Mm, Mp, Mfl, Mle	Climbing ripples (Mcl), mudstone drapes (Md), and flaser (Mfl) and lenticular bedding (Mle) within parallel-laminated (Mp) and massive-bedded mudstones (Mm)	Wave-dominated environment: backshore setting in which sediments were deposited within a swampy area. Root casts, reddish mottling, and caliche nodules represent palaeosol formation. Keller (1989), Miall (1996), Daidu et al. (2013)
Md, Mfl, Mle,	Mudstone drapes (Md), flaser (Mfl) and lenticular bedding (Mle)	Wave-dominated environment with strong tidal influence: backshore to nearshore setting in which Mle mostly forms in the supratidal (mudflat) and Mfl forms in the intertidal (sand flat) or alternatively in the subtidal if ripple crests are fully preserved. Keller (1989), Shanmugam (2003), Daidu et al. (2013)
Sct$_r$, Sct$_a$, Scr	Trough and tabular cross-beds (Sct$_r$, Sct$_a$) superimposed by current ripple marks (Scr), which record an opposite flow direction.	Wave-dominated environment with strong tidal influence: nearshore setting, deposits of (subtidal) sand dunes and sand waves. Baas (1978), Allen and Homewood (1984), Jost et al. (2016)
Sg, Shf, Sm, Sp, Sv	Pebbly lags (Sg), shell fragments (Shf) within massive- to parallel-laminated sandstones (Sm, Sp), occasionally with sand volcanoes (Sv)	Wave-dominated environment: foreshore to nearshore setting within the beach area, deposited in the surf-and-swash zone. Allen et al. (1985), Dam and Andreasen (1990), Keller (1990), Miall (1996), Jost et al. (2016)
Sbr, Scr, Sos, Sc, Sm, Sp	Ripple marks (Sbr, Scr, Sos) and cross-beds (Sc) within massive-bedded and parallel-laminated sandstones (Sm, Sp)	Wave-dominated environment: nearshore to foreshore setting in which ripple marks form beneath waves, while Sp form in the surf-and-swash zone (beach area). Baas (1978), Reineck and Singh (1980), Clifton and Dingler (1984), J. R. L. Allen (1984), Keller (1989, 1990)
Spw, Sc, Sos, Sm	Sandstone beds with a planar base and a wavy top (Spw), internally cross-bedded (Sc), superimposed by oscillation ripple marks (Sos) within massive-bedded sandstones (Sm)	Wave-dominated environment: nearshore to offshore setting, high-energetic storm deposits (tempestites). J. R. L. Allen (1982, 1984), Clifton and Dingler (1984), Miller and Komar (1980a, b), Diem (1986), Rust and Gibling (1990)

Table 2. Lithofacies encountered in the Napf units.

Facies assemblages	Structures and bedforms	Depositional setting and references
Gc, Gm	Cross- (Gc) and massive-bedded (Gm) conglomerates	Fluvial-dominated environment: megafan deposits within a braided river system. Gm and Gc form in active channels. Platt and Keller (1992), Schlunegger et al. (1997a)
Sc, Sm, Mp	Cross- (Sc) and massive-bedded (Sm) sandstones with parallel-laminated mudstones (Mp)	Fluvial-dominated environment: megafan deposits within a braided river system. Sc and Sm from crevasse splay deposits. Mp facies (often yellowish–reddish mottled with caliche nodules and root casts) is evident for palaeosol genesis on a floodplain. J. R. L. Allen (1982, 1984), Rust and Gibling (1990), Dam and Andreasen (1990), Keller (1990)

metres (Spw; Fig. 4a). Parallel-laminated (Sp) and massive-bedded (Sm) sandstone beds are decimetres thick and mainly found at the top of the OMM-Ib unit. Mudstones mostly occur as mudstone drapes (Md) on top of current ripple marks (Scr). Lenticular and flaser interbeds (Mle, Mfl) are decimetres thick and characterized by current ripple marks with truncated crests. The OMM-Ib then ends with a metre-thick mudstone displaying yellow to reddish mottling, root casts, and caliche nodules.

Estimates of palaeo-water depths (see the Supplement) reveal that the OMM-Ia sedimentary rocks were deposited in shallow conditions < 5 m deep (Fig. 4a and Table S2). At the base of the OMM-Ib palaeo-water depths were > 15 m and thus deeper compared to the OMM-Ia unit (see the Supplement). The OMM-Ib then shallows towards the top.

Measurements of the bedform orientations of the OMM-Ia deposits reveal sediment transport directions between 315° NW and 60° NE, with a dominant NE-directed transport (Fig. 4a). During OMM-Ib times, transport directions were bidirectional, and measurements reveal the full range between 260° W and 70° E (Fig. 4a). Dominant transport directions of the OMM-Ib sediments change towards the N and to the W up-section.

4.2 Proximal basin border in the centre: Napf units (site 12 in Fig. 2a)

The Napf units, which are a terrestrial interval of the OMM and the OSM (Fig. 3; Schlunegger et al., 1996), are ca. 1550 m thick and include a succession of conglomerates, sandstones, and mudstone interbeds (Matter, 1964), which we categorize into five lithofacies types (Table 2, Fig. S4d in the Supplement). Individual conglomerate beds are up to 10 m thick and display stacks of 2–3 m thick beds with massive- (Gm) to cross-bedded (Gc) geometries. The sandstone beds occur as massive-bedded (Sm) and cross-bedded (Sc) units. Interbedded mudstones are horizontally bedded (Mp) and have a yellowish–reddish mottling, caliche nodules, and root casts. Palaeo-flow measurements imply a change from a NE-directed transport during USM times to a NW-directed sediment transport between OMM-I and OSM times.

4.3 Proximal basin border to the west of the Napf: Sense section (site 7 in Fig. 2a)

The OMM at Sense (Figs. 4b and S4b) starts with a ca. 200 m thick succession of predominantly sandstones with some mudstone interbeds. Medium- to coarse-grained sandstone beds, up to 2–3 m thick, are massive-bedded (Sm), parallel-laminated (Sp), and trough cross-bedded (Sct$_r$) (Table 3). They also occur as metre-scale tabular cross-beds (Sct$_a$) forming several metre-thick sigmoidal foresets (Sc) with top and bottom sets and pebbly lags (Sg). These packages are well exposed along a nearby road-cut (Heitenried, Fig. 2a;

46°49′27″ N/7°18′42″ E; Fig. S4c in the Supplement). Some of these Sct$_r$ cross-beds contain current ripple marks (Scr), which are draped with a muddy layer (Md). Ripple marks also build up tabular sandstone bodies. They are either asymmetric (Scr) or symmetric (Sos) and may display branching crests (Sbr). In places, the sandstone bodies are highly bioturbated (Sf). Mudstone interbeds are 10–20 cm thick, massive- (Mm) to parallel-laminated (Mp), and strongly bioturbated (Mf).

The first occurrence of 5–10 m thick sandstone beds at the 200 m stratigraphic level (Fig. 4b) marks a distinct shift in the stratigraphic record where several metre-thick cross-bedded sandstone beds dominate the sedimentary succession. At this level, (i) 5–10 m thick normally graded sandstone beds overlie an erosive base and display epsilon cross-beds (Sce); (ii) cross-bedded sandstones (Sct$_a$) are several metres thick and tens of metres wide, and individual laminae sets are superimposed by current ripples (Scr) with an opposite flow direction than the cross-beds themselves; nearly all laminae sets of cross-beds (Sc) are superimposed by mudstone drapes (Md); and (iii) medium-grained sandstones display ridge-and-swale bedform geometries (Spw) with a small amplitude of a few decimetres and a large wavelength of several metres. Some of these Spw facies are occasionally covered with oscillation ripple marks (Sos). The Sense section ends with an alternation of decimetre-thick mudstone beds (Mm) and metre-thick massive- to cross-bedded conglomerates (Gm, Gc). These conglomerates then evolve towards an amalgamation of several metre-thick, massive-, and cross-bedded packages characterizing the uppermost ca. 50 m suite of the Sense section (Fig. 4b).

Estimates of palaeo-water depths range between 5 and 10 m (Fig. 4b and Table S4 in the Supplement) during the deposition of the lowermost 200 m. Conditions were deepest at the 200 m stratigraphic level, reaching water depths in the range of up to 30 m (see the Supplement). Measurements of sediment transport directions cover the range between ca. 0° N and 90° E (Fig. 4b) at the base of the Sense section, which then changed to an axial, bipolar SW–NE-directed transport and to a W-directed transport towards the end of the section (Fig. 4b).

4.4 Central basin: St. Magdalena site and Gurten drill core (sites 4 and 9 in Fig. 2a)

The sandstones within a cave system near Fribourg (St. Magdalena; Figs. 2a and S4c in the Supplement) are medium- to coarse-grained and display an amalgamation of up to 1–3 m wide cross-bedded troughs (Sct$_r$) with current ripple marks (Scr) at their base. The cross-bedded troughs and the ripple marks are both covered by mudstone drapes (Md). The amplitude of the troughs is in the range of several decimetres, whereas the cross-sectional widths span several decimetres to metres. The sandstones also occur as massive-bedded units (Sm). They are occasionally interbedded with current

Table 3. Lithofacies encountered in the Sense section.

Facies assemblages	Structures and bedforms	Depositional setting and references
Gm, Gc	Massive- to cross-bedded conglomerates (Gm, Gc)	Fluvial-dominated environment: terrestrial setting in which coarse-grained rivers deposited material. Platt and Keller (1992), Schlunegger et al. (1997a)
Sc, Sg, Sct$_r$, Sm	Cross-bedded sandstones (Sc) with top sets, foresets, and bottom sets with pebbly lags (Sg), associated with trough cross- (Sct$_r$) and massive-bedded sandstones (Sm)	Fluvial-dominated environment with tidal influence: foreshore setting in which deltas, or alternatively estuaries, enter the sea: Sc and Sg mark Gilbert delta-type deposits, while Sct$_r$ and Sm mark mouth bar deposits (or alternatively sand dunes). J. R. L. Allen (1982, 1984), Allen and Homewood (1984), Rust and Gibling (1990), Dam and Andreasen (1990)
Gm, Gc, Mm, Sm, Sg	Massive- to cross-bedded conglomerates (Gm, Gc) associated with massive-bedded sandstones and mudstones (Sm, Mm); occasionally, pebbles only occur as isolated layers within sandstones (Sg)	Tidal-dominated environment with fluvial influence (river inflow): nearshore setting. Terrestrial-derived material is washed into the subtidal setting by high-energetic floods. Dam and Andreasen (1990), Platt and Keller (1992), Miall (1996), Schlunegger et al. (1997a)
Mm, Mp, Mf	Massive-bedded (Mm) and parallel-laminated (Mp) mudstones with bioturbation (Mf)	Tidal-dominated environment: backshore setting, deposits of the supratidal (mudflat). Dam and Andreasen (1990), Keller (1990), Miall (1996)
Sm, Mm, Mf, Sf	Strongly bioturbated (Mf, Sf) massive-bedded mudstones and sandstones (Mm, Sm)	Tidal-dominated environment: backshore to foreshore setting, deposits of mud (supratidal) and sand flats (intertidal). Dam and Andreasen (1990), Keller (1990), Miall (1996), Nichols (1999)
Scr, Md, Sct$_a$, Sf	Current ripples (Scr) and tabular cross-beds (Sct$_a$) with mudstone drapes (Md), occasionally with heavily bioturbated sandstones (Sf)	Tidal-dominated environment: foreshore setting, deposits of the intertidal (sand flat), where bioturbation occurs (Sf). Mudstone drapes record slack-water phases. Baas (1978), Reineck and Singh (1980), Allen and Homewood (1984), Shanmugam (2003), Nichols (1999)
Sc, Sce	Cross-bedded (Sc) sandstones, occasionally forming epsilon cross-beds (Sce)	Tidal-dominated environment: foreshore to nearshore setting, deposits of a (meandering) tidal channel. J. R. L. Allen (1982, 1984), Frieling et al. (2009)
Sos, Sbr, Sp	Oscillation and branching ripple marks that grade into parallel-laminated sandstones	Tidal-dominated environment with strong wave influence: foreshore to nearshore setting, deposits of the beach area (surf-and-swash zone) and the wave transformation area. Reineck and Singh (1980), Clifton and Dingler (1984), J. R. L. Allen (1984), Keller (1990)
Sct$_a$, Scr, Md, Sct$_r$, Sm	Tabular (Sct$_a$) and trough cross-bedded (Sct$_r$) sandstones, superimposed with current ripples (Scr) and mudstone drapes (Md), associated with massive-bedded sandstones (Sm)	Tidal-dominated environment with fluvial influence (river inflow): foreshore to nearshore environment. Estuaries (Sct$_a$, Scr, Md) entering the sea, building up mouth bar deposits or alternatively subtidal sand dunes (Sct$_r$, Sm). Yalin (1964), Baas (1978), Allen and Homewood (1984), Dam and Andreasen (1990), Jost et al. (2016)
Sct$_r$, Scr, Md	Trough cross-beds (Sct$_r$) superimposed by current ripple marks (Scr) and mudstone drapes (Md)	Tidal-dominated environment: nearshore setting, deposits of (subtidal) sand dunes and sand waves. Baas (1978), Allen and Homewood (1984), Shanmugam (2003), Jost et al. (2016)
Spw, Sos, Sg	Sandstone beds with a planar base and a wavy top (Spw), superimposed by oscillation ripple marks (Sos) and embedded with pebbles (Sg)	Tidal-dominated environment with wave influence: nearshore to offshore setting, high-energetic storm deposits (tempestites). Reineck and Singh (1980), Miller and Komar (1980a, b), Clifton and Dingler (1984), Diem (1986), Miall (1996)

ripple marks (Scr) draped with mudstone layers (Md). Basal contacts are erosive. Measurements of morphometric properties (St. Magdalena; Fig. 2a) allow for an estimation of water depth, which is in the range of ca. 3 and 5 m (Table S1 in the Supplement). Sediment transport directions measured at the St. Magdalena site reveal a WSW–ESE-dominated sediment transport.

In the nearby ca. 260 m deep Gurten (Fig. 2a) drill core (Fig. S3 in the Supplement), OMM-Ia deposits occur as cross-bedded sandstones (Sc) topped with mudstone drapes (Md). These lithofacies associations (Table 4) are most abundant within the drill core and make up ca. 200 m of the log. However, because drill cores offer limited information about the dimensions of the encountered sediments, we were not able to determine if cross-beds can be assigned to tabular beds (Sct_a) or to troughs (Sct_r).

4.5 Basin axis in the west and the east: Lake Neuchâtel and Wohlen areas (sites 2 and 16 in Fig. 2a)

Calcareous, shelly sandstones (Scc) occur in the basin axis and are an assemblage of various lithofacies. This Scc facies association is made up of 5–10 m thick, coarse-grained sandstone beds with low-angle cross-beds (Sc) that contain coquinas, shell fragments (Shf), and pebbles (Sg) in places. Interbedded fine-grained sandstones contain current ripple marks (Scr) recording an opposite flow direction relative to the cross-beds (Sc).

In the west (sites at Lake Neuchâtel area; Figs. 2a and S4c in the Supplement), mapping shows that Scc Muschelsandstein deposits are ca. 5 m thick and record NNE- to NE-directed sediment transport. Foreset thicknesses of these deposits thin to < 1 m towards the front of the Napf megafan, where herringbone cross-beds imply SW- and NE-directed bimodal sediment transport. At the NE margin of the Napf, these Scc Muschelsandstein deposits grade into Slc Grobsandstein units, which show metre-thick tabular cross-beds (Sct_a) or decimetre-thick trough cross-beds (Sct_r) wherein individual troughs have metre-wide diameters. Measurements of palaeo-flow directions reveal a SW- and SE-directed transport. These deposits are either time-equivalent sediments of the Scc Muschelsandstein, and are thus contemporaneous with the OMM-Ib succession, or they mark the base of the OMM-II succession (Jost et al., 2016). Farther east near the Wohlen area (Figs. 2a and S4d in the Supplement), foresets of Muschelsandstein cross-beds are 6 to 8 m thick and in some locations up to 10 m thick as reported by Allen et al. (1985). Sediment transport directions were oriented towards the SSW, covering the range between 230° SSW and 250° WSW and striking parallel to the topographic axis. Estimates of the water depths of the Scc Muschelsandstein reveal palaeo-water depths (Table S1 in the Supplement) between 60 and 100 m.

5 Sedimentological interpretation

5.1 Entlen section

The OMM-Ia sedimentary rocks of the Entlen section are assigned to a backshore to upper nearshore realm within a wave-dominated environment (Fig. 4a, and please see Table 1 for references). Records of waves are inferred from (i) tabular, parallel-laminated and normally graded (Sp) sandstones, which are interpreted to represent sediments of the surf-and-swash zone near the wet beach where sedimentation occurs in the upper flow regime; (ii) low-angle cross-beds (Sc) with pebbly lags and shell fragments (Shf), which could reflect sand reefs (or shoals), rip channel fills, or storm layers; and (iii) oscillation (Sos) as well as branching ripple marks (Sbr) pointing to wave activity (Fig. 4a). Gravels and pebbly lags (Sg) are either evidence of high-energy storm events or river inflow from the backshore. Finer-grained lithofacies, which are either indicative of rapid sedimentation (Sv, Mcl; Table 1) or incipient pedogenesis (Mp, Mm; Table 1), are consistent with a shallow marine, wave-dominated environment.

The basal part of the OMM-Ib suite is assigned to a foreshore to lower nearshore setting shaped by the combined effect of wave and tidal activity (Fig. 4a). This is inferred by the observation that current ripple marks (Scr), which are situated on top of lamina sets of tabular (Sct_a) and trough cross-beds (Sct_r), point towards an opposite flow direction than the cross-beds themselves (Fig. 4a). Mudstone drapes (Md) on top of ripple marks, together with lenticular and flaser interbeds (Mle, Mfl), are supportive evidence for a tidal environment (references in Table 1). The occurrence of waves, however, is inferred from parallel-laminated sandstones (Sp) with parting lineations and ridge-and-swale (Spw) structures at the base of the OMM-Ib suite. At the top of the OMM-Ib, massive sandstones (Sm) and mudstones with mottled colours, root casts, and caliche nodules mark the presence of a backshore, possibly terrestrial setting.

The change from a nearshore, wave-dominated environment (OMM-Ia) to an environment with tidal records (OMM-Ib) was additionally associated with a deepening from < 5 to > 15 m at the base of the OMM-Ib, followed by a regressive sequence. We thus consider the base of this unit to be the maximum flooding surface (MFS), separating the OMM-I into a transgressive OMM-Ia unit and a regressive OMM-Ib succession (Figs. 4a and 5a).

5.2 Napf units

We interpret the association of massive- (Gm) to cross-bedded (Gc) conglomerates and massive- to cross-bedded sandstones (Sm, Sc) as deposits within a braided river system (Table 2; please see references there). In such an environment, conglomerates are common records of active channels. Massive- (Sm) to cross-bedded (Sc) sandstones alternating with mottled mudstones were most likely formed on the
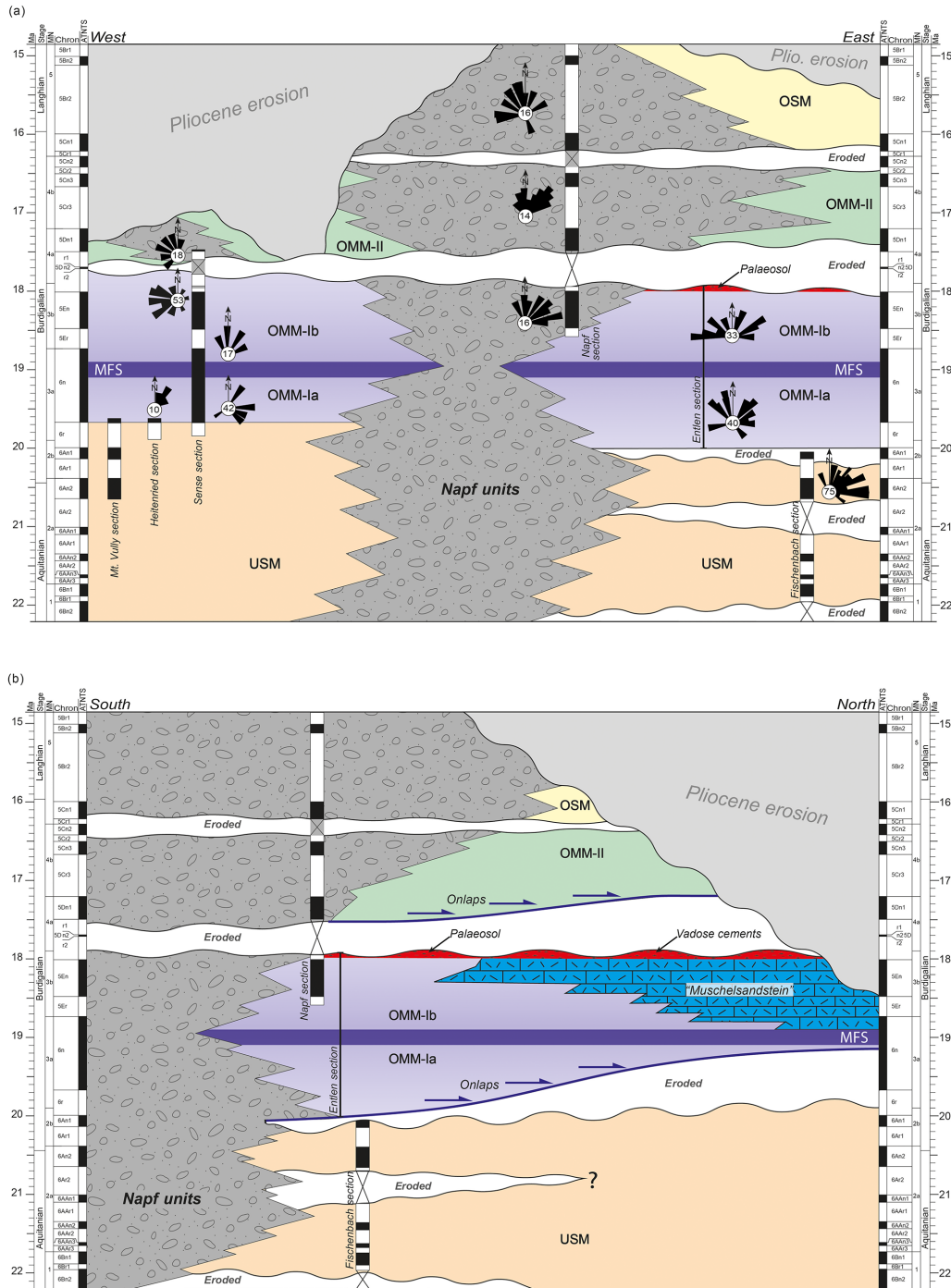
Figure 5. (a) West–east chronological (Wheeler) diagram of the Molasse sequence at the proximal basin border between Fribourg and Lucerne (Fig. 2a). The following magnetostratigraphic data have been used: Mt. Vully, Heitenried, and Sense (Strunck and Matter, 2002), as well as Napf and Fischenbach (Schlunegger et al., 1996). Palaeo-transport directions from Heitenried and the upper part of the Sense section are taken from Strunck and Matter (2002). Note that the Entlen section is not calibrated with magnetostratigraphic data but has been adjusted using regional information (see the text for further details and Fig. 3b for synthetic sections of the region). Note that Pliocene erosion removed most of the OMM-II record in western Switzerland. We infer marine conditions in the western Swiss Molasse basin during OMM-II times because (i) marine conditions were present east of the Napf units, and (ii) material transport occurred towards the west, which implies that marine conditions were also present west of the Napf megafan at that time as confirmed by mapping (e.g. Wanner et al., 2019). **(b)** North–south chronological (Wheeler) diagram of the Molasse sequence between Entlen (site 13) and Madiswil (site 14, both in Fig. 2a). See the text for further details. The onlaps (blue arrows) are based on interpretations from seismostratigraphic data (Schlunegger et al., 1997 TS4). MFS: maximum flooding surface.

Table 4. Lithofacies encountered at the St. Magdalena site and Gurten drill core.

Facies assemblages	Structures and bedforms	Depositional setting and references
Sct_r, Scr, Sc, Sm Md	Trough cross-beds (Sct_r) and cross-bedded sandstones (Sc) superimposed by current ripple marks (Scr) and mudstone drapes (Md), often associated with massive-bedded sandstones (Sm)	Tidal-dominated environment: nearshore setting, deposits of (subtidal) sand dunes (or mouth bar deposits) and megaripples; we infer these deposits as sediments of subtidal shoals. Baas (1978), J. R. L. Allen (1982, 1984), Allen and Homewood (1984), Rust and Gibling (1990), Dam and Andreasen (1990), Shanmugam (2003)

floodplains bordering the network of braided channels when bursts resulted in the accumulation of crevasse splay deposits (Platt and Keller, 1992). Mudstone interbeds (Mp) with evidence of palaeosol genesis formed when channel belts shifted away from the axis of the section (Platt and Keller, 1992). This facies association was mapped over tens of kilometres, both across and along strike of the basin orientation. It is thus assigned to an alluvial megafan (Schlunegger and Kissling, 2015), which was deposited by braided streams.

5.3 Sense section

We assign the OMM of the Sense section to a tidal-dominated environment in which deltaic estuaries dominated the sedimentary facies (Fig. 4b, and please see Table 3 for references). This is inferred from (i) sigmoidal cross-bedded sandstones (Sc) with distinct top sets, foresets, bottom sets, and pebbly lags (Sg) that are indicative of a delta and (ii) trough cross-bedded (Sct_r) and massive-bedded (Sm) sandstones that could represent mouth bar deposits where estuaries (or tidal inlets) end. In such environments, current ripple marks (Scr) with mudstone drapes (Md) at the base of tabular cross-beds (Sct_a) point to rhythmic changes in tidal current slack-water stages within a subtidal setting, whereas ripple marks (Sos) with branching crests (Sbr) and parallel-laminated sandstones (Sp) were most likely formed under the influence of waves close to the beach. Massive-bedded (Mm), parallel-laminated (Mp), and strongly bioturbated (Mf) mudstone interbeds are assigned to a tidal flat that established on the landside margin of the delta. Towards the top of the section, the facies successively evolves into a fan delta setting. This is inferred from the observation that the sedimentary suite thickens and coarsens upwards and ends with massive- to cross-bedded conglomerates (Gm, Gc), suggesting the progradation of a delta (e.g. Schaad et al., 1992).

The first occurrence of 5–10 m thick sandstone beds at the 200 m stratigraphic level (Fig. 4b) records a remarkable increase in the water depth when 5–10 m deep tidal channels (Sce sandstone beds with epsilon cross-beds) grade into several metre-thick subtidal sand waves (Sct_a) and nearshore tempestites (metre-scale Spw sandstones with ridge-and-swale geometries; see Table 3 for lithofacies and references).

These two latter lithofacies (Sct_a, Spw) are interpreted to record the deepest palaeo-water depth in the Sense section, when water depths were in the range of up to 30 m. We consider this stratigraphic level to record the maximum flooding surface (MFS) within the Sense section (Fig. 4b), and we will use it for correlation purposes with the OMM succession at Entlen (see the Discussion section).

5.4 St. Magdalena site and Gurten drill core

The several metre-thick outcrops near Fribourg are interpreted as subtidal shoal deposits, which accumulated within a tidal-dominated environment (Table 4; please see references there). This is inferred from metre-scale cross-bedded troughs (Sct_r) with current ripple marks (Scr) at their base (see also Homewood and Allen, 1981, for a similar interpretation). Alternatively, sandstone troughs (Sct_r) could be assigned to a mouth bar environment in which massive-bedded sandstones (Sm) would represent records of rapid sedimentation. In contrast, mudstone drapes (Md) on top of the ripple marks (Scr) and cross-beds (Sc) are formed during low-energy tides or possibly during slack stages. Similar deposits (Sct_r, or possibly Sct_a) within the Gurten drill core could also be interpreted as sediments of subtidal shoals; however, due to limited exposure, interpretations are non-conclusive. Shallow palaeo-water depths are also inferred from estimates of water depths ranging between 3 and 5 m.

5.5 Lake Neuchâtel and Wohlen areas

We interpret the Scc Muschelsandstein (Table 5) sediments (containing coquinas, shell fragments (Shf), and pebbles – Sg) to have been deposited within the topographic axis of the Burdigalian seaway (see also Allen et al., 1985, and Jost et al., 2016, for a similar interpretation). Metre-scale cross-beds (Sct_a), locally superimposed by current ripple marks (Scr), have been interpreted to reveal deposition under strong tidal currents (Allen et al., 1985). These deposits are thus assigned to offshore, tidal-dominated sand waves for which sediment transport was NNE- (Lake Neuchâtel area; Fig. 2a) or SSW-directed (Wohlen area, Fig. 2a). In places, pebbly lags (Sg) are interpreted as flood-related splays of gravels into the off-

shore setting, derived from the neighbouring Napf megafan. In contrast, the coarse-grained sandstones (Slc Grobsandstein sediments; Table 5) reveal similarities to the subtidal shoal deposits encountered at the St. Magdalena site where trough cross-bedded sandstones (Sct_r) and tabular cross-beds (Sct_a) dominate the facies assemblages. However, the deposits in the Wohlen area are coarser-grained, and cross-beds (Sc) have larger diameters but similar thicknesses. We relate the coarse-grained nature of these deposits to the proximity of the Napf megafan in the SW. The cross-beds with larger wavelengths and similar amplitudes possibly imply stronger currents compared to the subtidal shoal deposits near St. Magdalena.

6 Discussion

6.1 Reappraisal of chronostratigraphic framework

6.1.1 Entlen section

No magnetostratigraphic data are available for the Entlen section, but a temporal calibration of the deposits can be achieved through indirect lines of evidence. This particularly concerns the reconstruction of an age constraint for the basal transgression, which is accomplished using two lines of evidence: first, the transgression post-dates the deposition of the USM, which terminated at C6An1 at the Fischenbach section (Fig. 3b; Schlunegger et al., 1996). Second, based on stratigraphic interpretations of palaeo-flow direction data, Strunck and Matter (2002) considered the transgression of the OMM to have progressed from the east towards the west, where the first marine sediments have been dated with C6r in the Sense section (Fig. 3b; see next section). An E–W transgression of the OMM is also seen in seismic line BEAGBE.N780025 (Fig. S2 in the Supplement), where OMM deposits onlap the USM in a westward direction. Accordingly, the onset of the OMM at Entlen on the eastern side of the Napf predates the transgression at Sense farther west. Based on these arguments, we set an age of ca. 20 Ma for the base of the OMM-I in the eastern Swiss Molasse basin (Figs. 3b and 5), which is consistent with Kälin and Kempf (2009). For the top of the OMM-I, we determine an age using the magnetostratigraphy of the Napf section (Fig. 3b) ca. 10 km to the west of Entlen. This section includes an alternation of six reversed- and five normal-polarized magnetozones (Schlunegger et al., 1996). The lowermost, very long normally polarized interval (N1, Fig. 3b) includes the mammalian fossil site Hasenbach 1, recording an MN3b age (Schlunegger et al., 1996) and an even lower MN3b age, as a revision of the mammalian material has shown (Kälin and Kempf, 2009). This allows for a correlation of the normally polarized interval N1 with chron 5En of the MPTS (Cande and Kent, 1992, 1995) and the ATNTS (Lourens et al., 2004), respectively (Fig. 3b). Since the third reversed magnetozone of the Napf section is

very short (R2), and since the ATNTS chron 5D spans several hundred thousand years and is thus quite long, it is most likely that a hiatus encloses C5Dr2 to C5Dr1 (Fig. 3b). In addition, because (i) the change from MN3b to MN4a has been calibrated with C5Dr2 (Jost et al., 2016), and since (ii) the base of the overlying OMM-II (Figs. 3b and 5) has been dated with MN4 (Keller, 1989), we suggest that the inferred hiatus coincides with the boundary between the OMM-I and the OMM-II (Figs. 3b and 5). This age assignment is consistent with magneto-polarity stratigraphy in the Molasse basin ca. 70 km farther to the east (Kempf and Matter, 1999). It is also consistent with micro-mammalian investigations in the distal Molasse basin ca. 30 km farther north where Jost et al. (2016) found that deposits spanning MN3b and MN4a are missing. Based on these constraints, we suggest that the top of the OMM-I correlates with C5Dr of the MPTS and C5Dr2 of the ATNTS, respectively, followed by a ca. 0.5 Myr long hiatus (Figs. 3b and 5). According to this correlation, the sediments recording the maximum flooding conditions in the Entlen section are ca. 19 Myr old.

6.1.2 Wohlen area

Correlations of the OMM deposits from the Entlen section with the Wohlen area were accomplished by Schlunegger et al. (1997a) through a seismostratigraphic analysis of the seismic line 8307 (please see Fig. 2a for a trace of the line). The seismic data show that the OMM-I deposits onlap USM strata and then overlap this unit (Fig. 5b). Schlunegger et al. (1997a) correlated the OMM-I sequence with their Unit B in the Entlen section, which corresponds to the top of the OMM-Ia in our stratigraphic scheme. In addition, our field investigations and micro-mammalian data by Jost et al. (2016) revealed that the Muschelsandstein follows on top of the OMM-Ia and most likely corresponds in age to the OMM-Ib. Based on these arguments, we constrain the deposition in the distal basin to the time interval between ca. 19 and 18 Ma (Fig. 5b). However, based on seismostratigraphic investigations of line 8307, Schlunegger et al. (1997a) proposed that sedimentation was interrupted at ca. 18 Ma by a ca. 0.5 Myr long or possibly longer hiatus. This time span was later specified through new micro-mammalian discoveries by Jost et al. (2016), who noted that a record of MN4a is missing in the Wohlen area and that the base of the OMM-II hosts mammalian fragments that correspond to MN4b. The interpretation of an inferred unconformity is additionally supported through observations of vadose cements (Allen et al., 1985) within the Muschelsandstein and through evidence of a thick palaeosol separating OMM-I from OMM-II in the Entlen section (see Sects. 4 and 5). We use the occurrence of vadose cements and the palaeosol to propose that the uppermost beds of the OMM-Ib (including the Muschelsandstein) were exposed to erosion, or non-sedimentation, after deposition. Furthermore, because the Muschelsandstein unit records the deepest water depth

Table 5. Lithofacies encountered in the Lake Neuchâtel and Wohlen areas.

Facies assemblages	Structures and bedforms	Depositional setting and references
Scc, Sc, Scr, Shf, Sg	Calcareous, shelly sandstones (Scc; Muschelsandstein) are made up of cross-bedded sandstones (Sc) and contain co-quinas, shell fragments (Shf), and pebbles (Sg) in places.	Tidal-dominated environment: offshore setting, mega-sand waves deposited under strong tidal currents; pebbly lags (Sg) are interpreted as pebbles flushed into the sea by flood events. Baas (1978), Allen et al. (1985), Rust and Gibling (1990), Miall (1996), Jost et al. (2016)
Sct$_a$, Sct$_r$, Slc	Coarse-grained sandstones (Slc, Grobsandstein) with trough (Sct$_r$) and tabular (Sct$_a$) cross-bedded geometries	Tidal-dominated environment: nearshore to offshore setting, sand waves, or alternatively sand dunes, similar to the subtidal shoal deposits (see St. Magdalena site) but larger in diameter with similar thicknesses. Allen and Homewood (1984), Jost et al. (2016)

during OMM times at distal sites, we tentatively suggest that the deposition of these mega-sand waves started at the same time when the deepest conditions (MFS) were recorded within the Entlen section (Fig. 5b).

6.1.3 Sense section

Magnetostratigraphic data for the Sense section were presented by Strunck and Matter (2002). These authors placed the USM–OMM boundary at this site within C6r of the MPTS (Cande and Kent, 1992, 1995) or alternatively of the ATNTS (Fig. 3b; Lourens et al., 2004). The subsequent alternation of normal and reverse magnetozones was correlated by these authors with chrons 6r through 5Dn of Cande and Kent's MPTS (1992, 1995), the latter of which corresponds to C5Dn1 of the ATNTS (Lourens et al., 2004). Following Strunck and Matter (2002), a possible hiatus prior to ca. 17.7 Ma is also likely to be recorded within the Sense section (Figs. 3b and 5a). This correlation implies that the lower Sense Formation corresponds to the OMM-Ia, whereas the upper Sense Fm and the Kalchstätten Fm are time-equivalent units of the OMM-Ib (Fig. 3a and b). The topmost 50 m of the Kalchstätten Fm, with the base characterized by the first appearance of conglomerates, follows upon this hiatus and corresponds to the OMM-II in our scheme (Figs. 3 and 5a). This further implies that a hiatus separates OMM-I from OMM-II across the entire basin (Fig. 5a). In addition, subsequent sedimentation (base of OMM-II) progressed from the west to the east (Fig. 5a). In the same sense, the sediment packages recording the maximum flooding conditions (MFS) most likely have the same age across the entire basin (Fig. 5a).

6.1.4 Lake Neuchâtel area

No micro-mammalian sites have been reported for the OMM deposits in the distal western Molasse basin. Therefore, we cannot provide further constraints on the history of sedimen-

tation. However, our field inspections in the area of Lake Neuchâtel (Fig. 2a) show a sedimentary succession similar to that in the east, where amalgamated sandstone beds are overlain by the Muschelsandstein unit. Our field inspections also show that these calcareous, shelly sandstones thin from ca. < 10 m in the Lake Neuchâtel area in the west to a few metres towards the distal margin of the Napf megafan, consistent with the results by Allen et al. (1985). Because of the architectural similarity between the Muschelsandstein deposits in the east and the west, we tentatively consider the deposition of the Muschelsandstein to have occurred synchronously across the entire Swiss Molasse basin.

6.2 Evolution of the Molasse basin

The chronostratigraphic framework together with the sedimentological data and palaeo-flow directions are used to propose a scenario of how the basin evolved through time. During USM times (Fig. 6a), prior to the Burdigalian transgression, the basin was occupied by alluvial megafans at the proximal basin border, which gave way to an axially directed channel-belt system in the distal basin (Fig. 6a; Kuhlemann and Kempf, 2002). Analysis of heavy mineral assemblages by Füchtbauer (1964) and measurements of palaeo-flow directions in our study area (sole casts and cross-beds; this paper) and in eastern Switzerland (Kempf et al., 1999) revealed a NE-directed material transport towards the Munich region (Fig. 6a), which is consistent with the results of previous syntheses (e.g. Pfiffner et al., 2002; Kuhlemann and Kempf, 2002). In this area, the Molasse streams ended in a peripheral sea where neritic to open marine conditions prevailed (Kuhlemann and Kempf, 2002). Within the basin, a possible divide for sediment transport was situated somewhere SW of Geneva. We infer such a separation of sediment dispersal based on published sediment transport directions. In particular, south of Geneva, tidal cross-beds imply a sediment dispersal towards the south and thus towards the Tethys (Allen et al., 1991; Allen and Baas, 1993). To the northeast

of Geneva, however, our own measurements and data from Allen et al. (1985) reveal a NE-directed sediment transport to the Parathethys.

The palaeogeographic reconstruction based on our and published data for the period between ca. 20 and 19 Ma is shown in Fig. 6b. It illustrates that the central part of the Molasse basin changed to a shallow marine sea, which was ca. 40 km wide at that time. Our estimates of palaeo-bathymetric conditions and sedimentological data (Fig. 4a and b) reveal that the water depths corresponded to a subtidal and nearshore setting. Nearshore to possibly off-shore conditions (30–50 m) are recorded by subtidal mega-sand waves (Allen and Bass, 1993) south of Geneva and by the predominance of sandstone–mudstone alternations within the Boswil and Hünenberg drill cores in the NE (Wohlen area, Fig. 2a; Schlunegger et al., 1997a). Subtidal shoals, in up to 5 m deep water, occupied the western part of the central Swiss Molasse (Fig. 6b). This was already proposed by Homewood and Allen (1981), and it is confirmed here by our sedimentological data and estimates of palaeo-water depths (see the Supplement). Measurements of sediment transport directions from the shoal deposits reveal bimodal, SW–NE-directed transport with a dominant NE orientation. This is particularly the case at the proximal basin border near the Sense section (Fig. 2a) where deltaic fore-sets accumulated within an estuarine setting (Fig. 4b). Mapping of depositional settings allowed us to trace the shoal deposits towards the northern tip of the Napf megafan, from which the shoals narrow from ca. 20 to ca. 10 km over a 70 km long distance along strike. It thus appears that the shoals were deflected towards the topographic axis through a dominant NE-directed material transport (Fig. 6b). This interpretation is additionally supported by measurements of the transport directions of the Napf megafan (i.e. clast imbrications) and the coastal deposits at the Entlen section (i.e. parting lineation, cross-beds) pointing material transport towards the NE (Figs. 4a and 5a). At the distal margin of the basin, field inspections show that beach sandstones gave way to subtidal shoal deposits up-section. It thus appears that the Molasse basin between the Lake Neuchâtel and Wohlen areas (Fig. 2a) was a region of sediment export to the NE and to the SW. Material transport was most likely accomplished through strong tidal currents that entered the Swiss Molasse as two major tidal waves from the Tethys in the south and the Parathethys in the northeast (Bieg et al., 2008).

The situation during ca. 19–18 Ma (Fig. 6c) started with the time when the maximum flooding surface was formed in the depositional record (MFS; Fig. 5a and b). The sedimentological data reveal that this time was characterized by a widening of the basin to widths up to 80 km, and it was dominated by offshore conditions in the topographic axis with water depths > 50 m, as the Muschelsandstein deposits imply (Fig. 6c). There, cross-bed orientations (our measurements and data by Allen et al., 1985) and heavy mineral assemblages (Allen et al., 1985) reveal that sediment transport in the eastern basin axis (Wohlen area) occurred towards the SW, whereas sediment dispersal in the western basin axis (Lake Neuchâtel area) was directed towards the NE. We use this information to propose that a sedimentary depocentre established at the northern tip of the Napf megafan. In addition, this megafan is interpreted to have experienced a backstepping (see Sect. 6.3.3 for explanation). We infer such a scenario from the first appearance of a bimodal E–W orientation of material transport in the Entlen section (Fig. 5a). Because an E–W-oriented sediment transport requires a free passage for tidal currents along the southern basin margin, the seaside margin of the Napf megafan had to step back to allow such a passage to form (Fig. 6b and c).

The palaeogeographic situation shown in Fig. 6d comprises the time span between ca. 18 and ca. 14 Ma and displays the evolution from the OMM-II to the OSM. The OMM-II period followed a period of erosion and non-sedimentation across the entire Swiss Molasse basin, as our reassessment of the chronological framework of the OMM reveals (Fig. 5a and b). In addition, measurements of sediment transport directions reveal a SW-oriented sediment transport at proximal positions (Fig. 5a), which is consistent with the results of previous syntheses (e.g. Pfiffner et al., 2002; Kuhlemann and Kempf, 2002). This also implies that a possible E–W divide for sediment transport shifted towards the region near Munich or even farther east. Similar to Kuhlemann and Kempf (2002), we infer such a scenario from the supply of material with sources in the Hercynian basement north of Munich (Fig. 1a) or the Bohemian massif (Graupensandrinne, Fig. 6d; Allen et al., 1985; Berger, 1996; see also Sect. 2), which implies a westward tilt of the basin axis. This period ended with the progradation of the alluvial megafans during the time of the OSM.

In conclusion, this study confirms the results and syntheses of previous authors on the general sedimentation and material transport pattern during the deposition of the OMM. Nevertheless, our refinement of the chronological framework in combination with additional sediment transport data allow us to specify some further details on the development of the transgression of the OMM. These include (i) the establishment that the Burdigalian seaway was accompanied by both a deepening and widening of the basin. These mechanisms occurred contemporaneously and were associated with a northward shift of the topographic axis to the distal basin margin, where offshore and thus the deepest marine conditions established at 19 Ma. (ii) The reversal of the sediment transport direction from an originally NE-oriented sediment dispersal to a SW-oriented sediment transport started sometime after 20 Ma and was completed at 18 Ma at the latest. (iii) A wave-dominated coastline (with some tidal records) established on the eastern side of the Napf megafan (Fig. 4a), whereas a tidal-dominated estuarine environment characterized the proximal coastal margin on the western side of the Napf (Fig. 4b). These variations in sedimentation pattern ap-
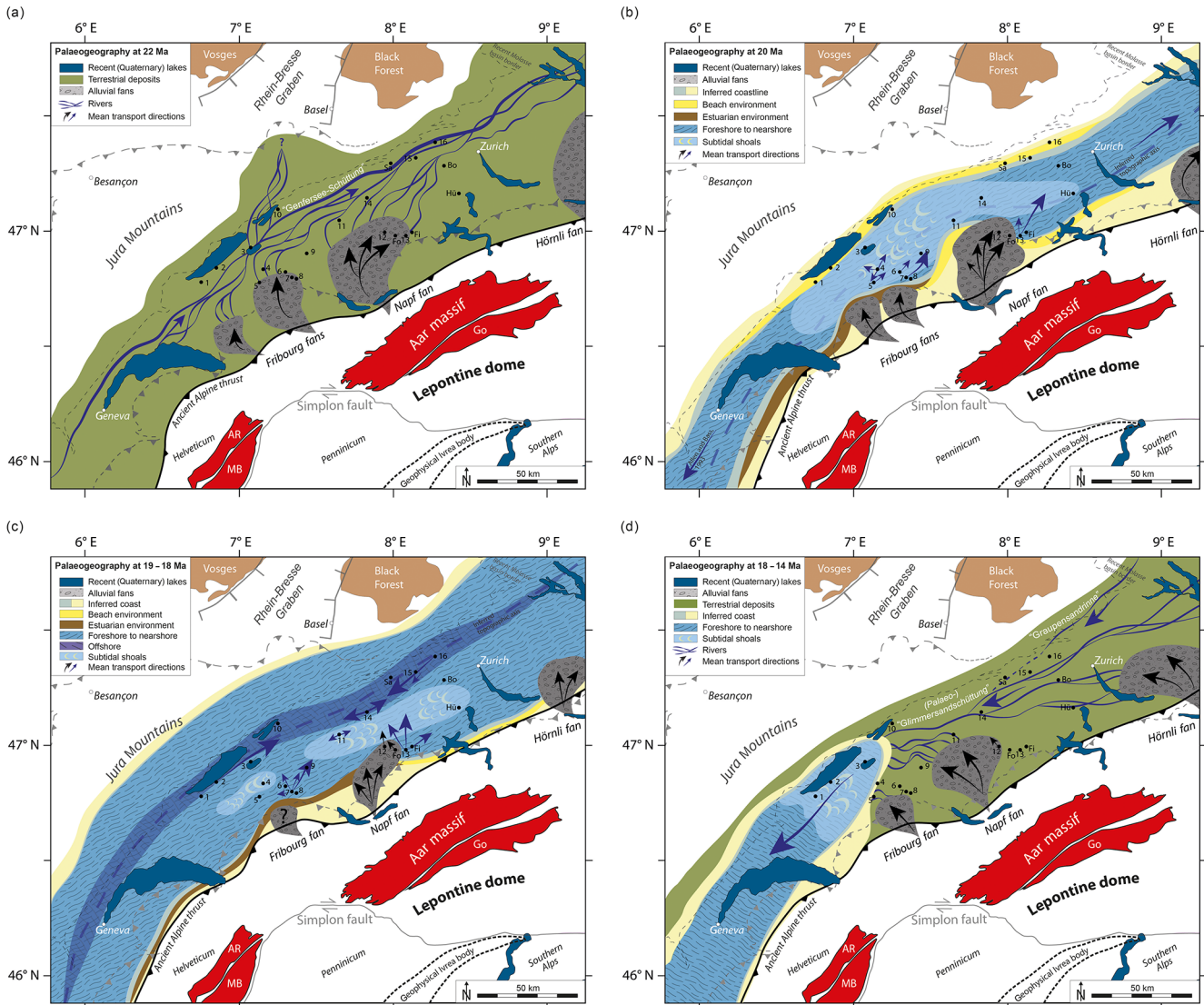
Figure 6. Palaeogeographical reconstructions of the Molasse basin at different stages: **(a)** USM (ca. 22 Ma), **(b)** OMM-Ia (ca. 20 Ma), **(c)** OMM-Ib (ca. 19–18 Ma), and **(d)** OMM-II to OSM (ca. 18 df TS5 –14 Ma) modified after Kuhlemann and Kempf (2002) and based on own observations. Note that all maps show present-day lithotectonic units within the Alps and the Jura Mountains for orientation purposes (dashed lines and grey lines). We acknowledge that the positions of these and the surface patterns (such as lakes) were different during the deposition of the Molasse deposits. The location of the palaeo-thrust fronts (thick lines) are adapted from Kuhlemann and Kempf (2002). Black dots mark study sites for orientation purposes. Please refer to Fig. 1 for the complete legend.

pear to explain why the lithostratigraphic framework differs between the two regions (see Fig. 3a).

6.3   Mechanisms associated with the transgression of the OMM

6.3.1   Reversal of the drainage direction

We relate the reversal of the drainage direction between the OMM-I and the OMM-II to tectonic processes operating at deeper crustal levels beneath the Alps. This interpretation is guided by Pfiffner et al. (2002), who related changes in sed-

iment dispersal within the Swiss part of the basin to a possible tilt of the foreland plate caused by the westward shift of the Ivrea body. This tectonic unit is comprised of mantle rocks with a high density (Fig. 1a) and thus could have influenced the deflection of the foreland plate (Pfiffner et al., 2002). While this mechanism is a viable explanation for the westward-directed tilt of the basin axis, we argue that a complementary driving force beneath the Eastern Alps is required to explain the drainage reversal across the entire basin, at least between Germany and Switzerland. We thus present a hypothesis of a possible geodynamic scenario to explain the

18 Myr old change in the drainage direction in the next section, but we also acknowledge that this interpretation is speculative at this stage and warrants further investigations. Such an exploration, however, requires the geodynamic processes between 33 and 30 Ma to also be considered. At that time, the subducted European oceanic lithosphere was considered to have broken off beneath the Central Alps (Davies and von Blanckenburg, 1995; Schmid et al., 1996). However, underneath the Eastern Alps the European oceanic lithosphere remained attached to the continental plate as palinspastic restorations revealed (Handy et al., 2015). The consequence was the rise of the Alpine topography and a large sediment flux to the Swiss Molasse basin (Sinclair, 1997; Kuhlemann et al., 2001a, b; Willett, 2010; Garefalakis and Schlunegger, 2018), which became overfilled at ca. 30 Ma (Sinclair and Allen, 1992; Sinclair, 1997; see also Sect. 2.1). East of Munich, however, the basin still remained underfilled until ca. 20 Ma as evidenced by deep marine sedimentation, whereby debris flows and proximal turbidites accumulated within the basin axis (Fertig et al., 1991; Malzer et al., 1993). We use these observations to propose that vertically directed slab load forces were still downwarping the foreland plate beneath the Eastern Alps to allow such a deep trough to form. In contrast, slab break-off beneath the Central Alps most likely caused a rebound of the foreland plate in Switzerland (Schmid et al., 1996; Schlunegger and Castelltort, 2016). We interpret the consequence to be a stronger downward deflection of the European foreland plate beneath the Eastern Alps compared to the Central Alps, which could explain the east-directed sediment transport prior to ca. 20 Ma (Fig. 6a).

Between ca. 20–17 Ma, i.e. during OMM times, a remarkable change was recorded in the Molasse basin. The eastern Molasse basin experienced a change from deep to shallow marine conditions (Kuhlemann and Kempf, 2002), and the entire basin recorded a reversal of the drainage direction from the E to the W (see above). We relate these shifts to a change in the pattern of slab load forces underneath the Eastern and Central Alps. Particularly in the eastern Molasse basin, the change from deep to shallow marine conditions could reflect a response to slab unloading through delamination, or break-off, of the subducted European lithosphere underneath the Eastern Alps (Ustaszewski et al., 2008), while rollback subduction of the European plate beneath the Central Alps of Switzerland continued, as Kissling and Schlunegger (2018) proposed. This could have resulted in a rebound of the European plate beneath the Eastern Alps, whereas plate downwarping continued beneath the Central Alps. We interpret these along-strike differences in the plate deflection to have caused a westward tilt of the foreland plate, which in turn could have controlled the drainage reversal. The reasons for the along-strike differences in the subduction mechanisms are not clear at this stage and could either be related to (i) inheritance related to the Mesozoic phase of rifting (Schmid et al., 2004; Handy et al., 2010) or (ii) differences in the mechanical strengths and rheological conditions of the foreland

plate between the Swiss and the German–Austrian Molasse basins (Tesauro et al., 2009, 2013).

6.3.2 Widening of the basin

The drainage reversal occurred simultaneously with the widening of the basin in central Switzerland, as our chronological refinement shows. Because both changes occurred at the same time, one could infer a causality of the underlying controls. We refrain from such a view at this stage since we lack a detailed 3-D restoration of the tectonic and geodynamic situation of the Alps–Molasse basin system for that time. Nevertheless, a possible control on the widening of the basin can be identified based on a cross-sectional view across the Central Alps and the related geodynamic processes during the Burdigalian ca. 20 Myr ago (Fig. 7). At that time, we propose that the velocity of rollback subduction beneath the Central Alps of Switzerland was likely to have accelerated. We justify this interpretation through the observation that (i) tectonic exhumation of the Lepontine dome (Fig. 1), accomplished through slip along the Simplon detachment fault (Mancktelow and Grasemann, 1997), occurred at the highest rates at that time (Boston et al., 2017; Schlunegger and Willet, 1999) and that (ii) the rapid rise of the Aar massif (Fig. 1) also commenced at 20 Ma (Herwegh et al., 2017). Following the concepts of Kissling and Schlunegger (2018), these processes require a mechanism whereby buoyant crustal material several tens of kilometres thick was delaminated from the subducting European continental plate and accumulated within the crustal root (Fig. 7) within a short time period. In agreement with Kissling and Schlunegger (2018), we interpret a rapid phase of rollback subduction as also being able to shift the basin axis to more distal sites. We use these mechanisms to explain the cross-sectional widening of the Molasse basin at 19 Ma and the northward shift of the basin axis (Fig. 7), thereby giving way to the deposition of the offshore Muschelsandstein (Fig. 6b and c). This lithofacies association has been mapped along the distal basin border adjacent to the external massifs only.

6.3.3 Uplift of the Aar massif and establishment of a wave-dominated coast in the east and tidal records in the west

We interpret the different coastal morphologies between the eastern and western sides of the Napf megafan (see Sect. 5) to have rather been controlled by tectonic processes than by contrasts between the tidal waves from the Paratethys and the Tethys. We tentatively exclude a surface control at this stage because the pattern of tidal sand waves in the basin axis is not reflected by a corresponding coastal morphology at the proximal basin margin. In particular, the Muschelsandstein cross-beds are thicker in the Wohlen area (up to 10 m) than in the Neuchâtel region (< 10 m; see Sects. 4 and 5 and the Supplement), implying stronger shear velocities in the east-

Situation of the Alps at c. 20 – 18 Ma

Mod. after Schlunegger and Kissling (2015) and Kissling and Schlunegger (2018)
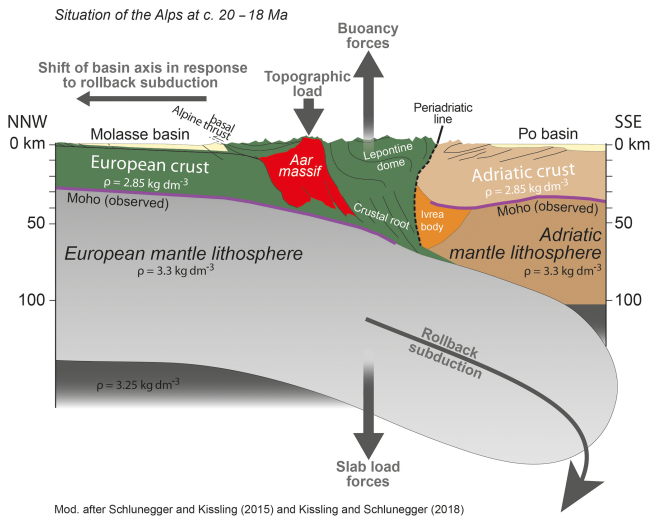
Figure 7. Simplified geological–geophysical model of the Alpine orogen for the time between 20 and 18 Ma, showing the most important geodynamic forces that might have shaped the Molasse basin and induced the transgression. Modified after Schlunegger and Kissling (2015) and Kissling and Schlunegger (2018).

ern basin axis compared to the west. At the proximal basin margin, however, the coastal deposits on the eastern side of the Napf predominantly record the activities of waves, while compelling evidence of tidal activities is more abundant to the west of the Napf megafan. Instead, because the establishment of wave- and tidal-dominated shorelines occurred contemporaneously with the rise of Aar massif (Herwegh et al., 2017), we interpret this tectonic event to have possibly influenced the distribution of the depositional settings at the proximal basin border. In particular, as we explain in the following paragraphs, the rise of the Aar massif is likely to have resulted in a shift of surface loads (Fig. 7) and in a buckling of the foreland plate, which possibly influenced the water depths and the distribution of facies.

Structural mapping in the Aar massif (Wehrens, 2015; Wehrens et al., 2017) has revealed that crustal blocks were rising along steeply SE-dipping thrust faults (Fig. 1b). This process was related to rollback subduction of the European mantle lithosphere and the related delamination of crustal material, which resulted in the rise of the Aar massif (Herwegh et al., 2017; Fig. 1b). This mechanism also lifted the topography surrounding the massif to higher elevations (Fig. 7), thereby forming a positive anomaly in the topographic load in the region. Sinclair et al. (1991) and Sinclair (1996) explored a possible stratigraphic response to topographic loading associated with the uplift of the Aar massif (Sinclair et al., 1991) through the application of a linear elastic plate model where thrusting and erosion are dynamically coupled. In their model, the distance between the location of thrusting (Aar massif) and the site in the basin wherein a signal is expected depends primarily on the flexural rigid-

ity (or alternatively the elastic thickness or the Te value) of the crustal rocks underlying the foreland basin (Sinclair, 1996). The flexural rigidity of the rocks beneath the Swiss Molasse basin has been quantified with an elastic thickness of ca. 10 km using stratigraphic constraints (Sinclair et al., 1991). This estimate is particularly based on thickness gradients of accumulated Molasse deposits across a section from the distal basin border to the Alpine thrust front. This pattern, however, could have been influenced by upper crustal inhomogeneities (Waschbusch and Royden, 1992) such as pre-existing faults (Pfiffner, 1986). This could explain why estimates of Te values that are based on stratigraphic data are lower (Sinclair et al., 1991; Schlunegger et al., 1997b) than estimates that are based on the curvature of the entire European foreland plate from the distal Molasse border to the core of the Alps and even deeper (Pfiffner et al., 2002; Schlunegger and Kissling, 2015), where Te values up to 50 km have been proposed (see the discussion in Pfiffner et al., 2002). However, because the flexural response of the Molasse basin to local topographic loads was likely to have been influenced by inherited faults in the basement (Pfiffner, 1986), lower Te values appear more appropriate (Waschbusch and Royden, 1992). Accordingly, if we consider a local and thus upper crustal response to loading characterized by a Te value of ca. 10 km (Sinclair et al., 1991; Schlunegger et al., 1997b), then shifts in surface loads through the kilometre-thick stacking of additional material in the Aar massif are likely to have resulted in the formation of several tens of metres of supplementary accommodation space at the proximal basin border, as the models of Sinclair et al. (1991) predict. As a result, depocentres in the Molasse basin are predicted to step back to proximal positions (Sinclair et al., 1991), which is consistent with our interpretation of the flow directions and the inferred backstepping of the Napf megafan (see Sect. 6.1 and Fig. 6). In addition, according to Sinclair (1996), upward-directed bulging of a few tens of metres is expected at the distal (forebulge) and at the lateral margins of the load (lateral bulge). The spacing between an expected lateral bulge and the location of the surface forcing ranges between 50 and 100 km (using a Te value of 10 km), which is consistent with the distance between the Aar massif and the inferred subtidal shoals in the western Swiss Molasse basin (near Fribourg; Figs. 2a and 6b). Accordingly, we suggest that the establishment of subtidal shoals at the northern tip and on the western side of the Napf is the consequence of this bulging (Fig. 6b and c). Because the plate had an eastward tilt at that time, as inferred from palaeo-flow directions, such a flexural signal could possibly not be recorded on the eastern side of the Aar massif where the marine conditions were too deep (Fig. 6b and c).

We additionally use these mechanisms to explain the development of different depositional settings at the proximal basin border of the Swiss Molasse basin. East of the Napf megafan, a relatively high subsidence (rate of ca. 340 m Ma^{-1} [TS6] for OMM-Ia and ca. 430 m Ma^{-1} for

OMM-Ib; based on data in Fig. 4a) most likely resulted in a steeper submarine gradient compared to the west, where the inferred bulging possibly lowered and subdued the submarine slopes (subsidence rate of ca. 285 m Ma^{-1} for both OMM-Ia and OMM-Ib; based on data in Fig. 4b). This could explain why the evidence of wave action is predominantly recorded along the eastern proximal steeper basin margin. Indeed, investigations on modern coasts have shown that steeper coasts tend to promote the formation of larger waves (Flemming, 2011). In contrast, in the western Swiss Molasse, estuaries and tidal channels could develop as the wave energy decreased in the subdued coastal landscape. Note that we cannot fully exclude the possibility that uplift along basement faults beneath the Molasse basin in western Switzerland (Spicher, 1980) shifted the peripheral sea to shallow water depths during OMM times. If such a mechanism did occur, then it could have amplified the effects related to flexural bulging.

6.3.4   Controls influencing changes in sediment supply

The time around 20 Ma was also characterized by a continuous reduction in sediment flux from originally 25 000 km^3 Ma^{-1} prior to ca. 20 Ma to ca. 15 000 km^3 Ma^{-1} thereafter (Kuhlemann, 2000; Kuhlemann et al., 2001a, b), which could have contributed, together with the tectonic widening of the basin, to the transgression of the peripheral sea in Switzerland (Fig. 8). The mechanisms leading to this reduction in surface mass flux are not fully understood (Kuhlemann et al., 2002) and multiple hypotheses have been proposed, including the following: (i) shifts towards a dryer palaeoclimate paired with a widespread exhumation of crystalline rocks with low bedrock erodibilities (Schlunegger et al., 2001); (ii) tectonic exhumation of the Lepontine through slip along the Simplon detachment fault, which occurred in response to rapid rollback subduction (see above and Kissling and Schlunegger, 2018) – tectonic exhumation was considered to have shifted the drainage divide farther to the north, thereby substantially decreasing the source area of the Molasse basin (Kuhlemann et al., 2001a); and (iii) uplift of the Aar massif, which was considered to have resulted in a reorganization of the Alpine streams and which was also associated with a reduction of the source area of the Molasse basin (Kühni and Pfiffner, 2001). Except for the palaeoclimate hypothesis, all other mechanisms are ultimately linked to the tectonic processes we have outlined in the sections above.

6.3.5   Controls related to changes in eustatic sea level

Whereas tectonic processes are recorded in the arrangement of depositional settings in the entire Swiss Molasse basin, signals related to the eustatic changes in sea level are possibly recorded by several hiatuses. This particularly concerns the times of non-sedimentation between OMM-I and OMM-
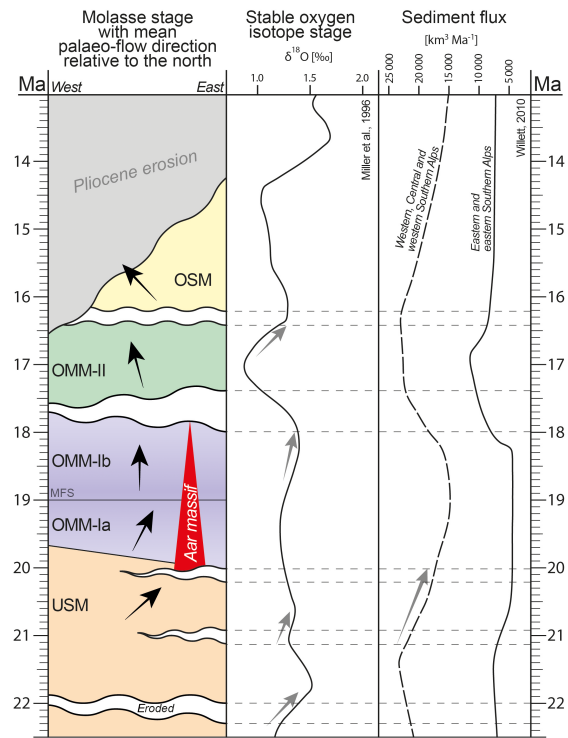
Figure 8. Molasse stages (USM, OMM, and OSM) with mean palaeo-transport directions (black arrows), hiatuses plotted against stable oxygen isotope stages (Miller et al., 1996), and sediment flux (Kuhlemann, 2000; Willet, 2010). The red triangle demarcates the onset of delamination and rapid exhumation of the Aar massif (Herwegh et al., 2017). Grey arrows demarcate decreases in sediment flux and falls in the eustatic sea level, possibly contributing to the related hiatuses. MFS: maximum flooding surface.

II and between the OMM and the OSM phase, which we have elaborated on in Sect. 5.1 (Figs. 5a and 8). In this context, δ^{18}O values measured on benthic foraminifera have been used as proxy for establishing patterns of sea level changes (Miller et al., 1998). In particular, a shift to more positive values of the stable oxygen isotope δ^{18}O implies the growth of polar ice sheets, where lighter oxygen isotopes (δ^{16}O) are preferentially stored (Zachos, 2001). As a consequence, global sea level most likely decreased (the amplitude of the drop is not really known) during shifts towards heavier (and thus more positive) isotopic records in planktonic organisms (Miller et al., 1998). These patterns have been reconstructed by Miller et al. (1996, 1998) at a high resolution. Shifts towards larger δ^{18}O values generally coincide with times when hiatuses are recorded in the Molasse basin (Fig. 8; see also Pippèrr and Reichenbacher, 2017; Sant et al., 2017). We thus suggest that drops in global sea level of a few tens of metres initiated a phase of non-deposition in the Swiss part of the Molasse basin, at least between OMM-I and OMM-II at ca. 18 Ma and between the OMM and the OSM. In contrast, phases of deposition appear to have occurred during periods

when the global sea level was high. This was most likely the case during the deposition of the OMM-II at ca. 17 Ma when the isotope data imply that the sea reached a maximum eustatic level, at the least during the Burdigalian (Fig. 8). We acknowledge that a rising sea level could also have contributed to the transgression of the OMM-I and the establishment of the maximum flooding surface (MFS), but the amplitude of change is much less compared to the OMM-II. Instead, we consider the reduction in sediment flux and the changes in tectonic processes to have been exerting a stronger control.

7 Summary and conclusion

In summary, we suggest that the Burdigalian transgression was related to a combination of a deepening and widening of the basin and a reduction of sediment supply rates, which we ultimately relate to tectonic processes in the Alpine hinterland. In this context, we consider rollback subduction to have most likely been responsible for the widening of the basin in the foreland and for the shift of the basin axis to distal positions. In addition, rollback subduction of the European mantle lithosphere and delamination of crustal material most likely resulted in the rapid exhumation of the Lepontine dome (Boston et al., 2017) and the associated rise of the Aar massif (Herwegh et al., 2017). These processes are interpreted to have triggered the change in the configuration of the drainage network (Schlunegger et al., 2001; Kühni and Pfiffner, 2001), with the consequence that the sediment flux to the basin decreased. This reduction in sediment flux, together with the tectonic widening of the basin, was thus likely to have shifted the basin to underfilled conditions, which could have allowed the transgression of the peripheral sea in Switzerland (Fig. 8). In addition, shifts in surface loads, caused by the rise of the Aar massif, resulted in flexural adjustments in the Molasse basin through the buckling of the foreland plate. We suggest that this influenced the water depths within the basin, which could explain the development of distinct depositional settings and the formation of subtidal shoals wherein a lateral bulge is expected. Because of the formation of shallow marine conditions, subtle changes in eustatic sea level contributed to the occurrence of several hiatuses (Sant et al., 2017). Whereas these mechanisms are capable of explaining the establishment of the Burdigalian seaway and the formation of distinct sedimentological niches in Switzerland, the drainage reversal during OMM times possibly requires a change in the tectonic processes at a scale that includes the subduction history of the entire mountain range, at least between the Eastern and Central Alps. Current explanations are still speculative and await the results of ongoing research in the framework of the AlpArray initiative. At this stage, we conclude that the geodynamic processes in the Alps include subduction mechanisms, delamination of crustal material, the uplift of the Aar massif, reorganization of the drainage network, and lower sediment fluxes, which are reflected in the Swiss Molasse basin through the establishment of shallow marine conditions and a shift of the topographic axis towards more distal sites at 19 Ma. Accordingly, the Burdigalian transgression in Switzerland most likely had a tectonic driving force but with amplifications through responses occurring on the surface of the Alps and the Molasse basin.

Data availability. The dataset is available from the senior author upon request.

Supplement. The supplement related to this article is available online at: https://doi.org/10.5194/se-10-1-2019-supplement. TS7

Author contributions. FS designed the study. PG CE2 carried out the experiments and collected and interpreted the data with support by FS. The figures and photos were created by PG with support by FS. FS and PG wrote the text. TS8

Competing interests. The authors declare that they have no conflict of interest.

Acknowledgements. This research was funded through the Swiss National Science Foundation. Special thanks go to Kenneth Eriksson, Kei Ogata, and an anonymous reviewer for their constructive and insightful comments. The supportive editorial handling by Elias Samankassou is kindly acknowledged. We would also like to thank SEAG (Aktiengesellschaft für Schweizerisches Erdöl), who provided us with a scan of the seismic line BEAGBE.N780025, and Kellerhals and Haefeli AG for permission to use the photos of the Gurten drill core.

Financial support. This research has been supported by the Swiss National Science Foundation (grant no. 154198). TS9

Review statement. This paper was edited by Elias Samankassou and reviewed by Kei Ogata, Kenneth Eriksson, and one anonymous referee.

References

Allen, J. R. L.: Sedimentary Structures. Their Characteristics and Physical Basis. Vol. I, Developments in Sedimentology 30A, Elsevier, Amsterdam, 593 pp., 1982.

Allen, J. R. L.: Sedimentary Structures. Their Characteristics and Physical Basis. Vol. I., Developments in Sedimentology 30B, Elsevier, Amsterdam, 679 pp., 1984.

Allen, P. A.: Reconstruction of ancient sea conditions with an example from the Swiss Molasse, Mar. Geol., 60, 455–473, 1984.

Allen, P. A.: Earth Surface Processes, 404 pp. ISBN 0-632-03507-2, 1997. TS10

Allen, P. A. and Allen, J. R.: Basin Analysis: Principles and Applications, Malden, MA, Blackwell Pub., ix, 549 pp., ISBN: 0632052074, 2005.

Allen, P. A. and Bass, J. P.: Sedimentology of the Upper Marine Molasse of the Rhône-Alp region. Eastern France: Implications for basin evolution. Eclogae Geol. Helv., 86, 121–171, 1993.

Allen, P. A. and Homewood, P.: Evolution and mechanics of a Miocene tidal sandwave, Sedimentology, 31, 63–81, 1984.

Allen, P. A., Mange-Rajetky, A., and Matter, A.: Dynamic palaeogeography of the open Burdigalian seaway, Swiss Molasse basin, Eclogae Geol. Helv., 78, 351–381, 1985.

Allen, P. A., Crampton, S. L., and Sinclair, H. D.: The inception and early evolution of the North Alpine foreland basin, Switzerland, Basin Res., 3, 143–163, 1991.

Baas, J. H.: Ripple, ripple mark, ripple structure. In: Sedimentology. Encyclopedia of Earth Science, Springer, Berlin, Heidelberg, 921–925, 1978.

Baran, P., Jodłowski, G. S., Krzyżanowski, A., and Zaręba, K.: Experimental testing of methanol sorption on selected coal samples from Upper Silesian Basin, Geology, Geophysics and Environment, 40, 261–269, 2014.

Beaumont, C.: Foreland basins, Geophys. J. Int., 65, 291–329, 1981.

Berger, J.-P.: Cartes paléogéographiques-palinspastiques du bassin molassique suisse (Oligocène inférieur – Miocène moyen), N. Jb. Geol. Paläont. Abh., 2002, 1–44, 1996.

Bieg, U., Süss, M. P., and Kuhlemann, J.: Simulation of tidal flow and circulation patterns in the Early Miocene (Upper Marine Molasse) of the Alpine foreland basin, Analogue and Numerical Modelling of Sedimentary Systems: From Understanding to Prediction, 40, 145–169, 2008.

Boston, K. R., Rubatto, J., Hermann, J., Engi, M., and Amelin, Y.: Geochronology of accessory allanite and monazite in the Barrovian metamorphic sequence of the Central Alps, Switzerland, Lithos, 286–287, 502–518, 2017.

Bridge, J. S. and Tye, R. S.: Interpreting the dimensions of ancient fluvial channel bars, channels and channel belts from wireline-logs and cores, AAPG Bull., 84, 1205–1228, 2000.

Cande, S. C. and Kent, D. V.: A new geomagnetic polarity time scale for the Late Cretaceous and Cenozoic, J. Geophys. Res., 97, 913–951, 1992.

Cande, S. C. and Kent, D. V.: Revised calibration of the geomagnetic polarity timescale for the Late Cretacesou and Cenocoic, J. Geophys. Res., 100, 6093–6095, 1995.

Cederbom, C. E., Sinclair, H. D., Schlunegger, F., and Rahn, M.: Climate-induced rebound and exhumation of the European Alps, Geology, 32, 709–712, 2004.

Cederbom, C. E., van der Beek, P., Schlunegger, F., Sinclair, H. D., and Oncken, O.: Rapid extensive erosion of the North Alpine foreland basin at 5–4 Ma, Basin Res., 23, 528–550, 2011.

Clifton, H. E. and Dingler, J. R.: Wave-Formed Structures and Paleoenvironmental Reconstruction, Mar. Geol., 60, 165–198, 1984.

Daidu, F., Yuan, W., and Min, L.: Classifications, sedimentary features and facies associations of tidal flats, J. Palaeogeogr., 2, 66–80, 2013.

Dam, G. and Andreasen, F.: High-energy ephemeral stream deltas; an example from the Upper Silurian Holmestrand Formation of the Oslo Region, Norway, Sediment. Geol., 66, 197–225, 1990.

Davies, J. and von Blanckenburg, F.: Slab breakoff: A model of lithosphere detachment and its test in the magmatism and deformation of collisional orogens, Earth Planet. Sc. Lett., 129, 85–102, 1995.

DeCelles, P. G.: Late Jurassic to Eocene evolution of the Cordilleran thrust belt and foreland basin system, western USA, Am. J. Sci., 304, 105–168, 2004.

DeCelles, P. G. and Giles, K. A.: Foreland basin systems, Basin Res., 8, 105–123, 1996.

Diem, B.: Analytical method for estimating paleowave climate and water depth from wave ripple marks, Sedimentology, 32, 705–720, 1985.

Diem, B.: Die Untere Meeresmolasse zwischen der Saane (Westschweiz) und der Ammer (Oberbayern), Eclogae Geol. Helv., 79, 493–559, 1986.

Doppler, G.: Zur Stratigraphie der nördlichen Vorlandmolasse in Bayerisch-Schwaben, Geologica Bavarica, 94, 83–133, 1989.

Fertig, J., Graf, R., Lohr, H., Mau, J., and Müller, M.: Seismic sequence and facies analysis of the Puchkirchen Formation, Molasse basin, south-east Bavaria, Germany, Eur. Assoc. Pet. Geosci. Spec. Publ., 1, 277–287, 1991.

Flemings, P. B. and Jordan, T. E.: Stratigraphic modeling of foreland basins: Interpreting thrust deformation and lithosphere rheology, Geology, 18, 430–434, 1990.

Flemming, B. W.: Geology, Morphology, and Sedimentology of Estuaries and Coasts, Treatise on Estuaries and Coasts, 3, 7–38, 2011.

Frieling, D., Mazumder, R., and Reichenbacher, B.: Tidal sediments in the Upper Marine Molasse (OMM) of the Allgäu area (Lower Miocene, Southwest-Germany), Neues Jahrb. Geol. P.-A., 254, 151–163, 2009.

Froitzheim, N., Schmid, S. M., and Frey, M.: Mesozoic paleogeography and the timing of eclogite-facies metamorphism in the Alps: A working hypothesis, Eclogae Geol. Helv., 89, 81–110, 1996. TS11

Fry, B., Deschamps, F., Kissling, E., Stehly, L., and Giardini, D.: Layered azimuthal anisotropy of Rayleigh wave phase velocities in the European Alpine lithosphere inferred from ambient noise, Earth Planet. Sc. Lett., 297, 95–102, 2010.

Füchtbauer, H.: Sedimentpetrographische Untersuchungen in der älteren Molasse nördlich der Alpen, Eclogae Geol. Helv., 61, 157–298, 1964.

Garefalakis, P. and Schlunegger, F.: Link between concentrations of sediment flux and deep crustal processes beneath the European Alps, Sci. Rep.-UK, 8, 183, 2018. TS12

Haldemann, E. G., Haus, H. A., Holliger, A., Liechti, W., Rutsch, R. F., and Della Valle, G.: Geologischer Atlas der Schweiz, Blatt 1188 Eggiwil (Nr. 75): Schweizerische Geologische Kommission, scale 1 : 25 000, 1 sheet, 1980.

Hammer, B.: Sedimentologie der Oberen Meeresmolasse im Raum St. Gallen, unpublished Diploma thesis, Univ. Bern, Bern, Switzerland, 96 pp., 1984.

Handy, M. R., Schmid, S. M., Bousquet, R., Kissling, E., and Bernoulli, D.: Reconciling plate-tectonic reconstructions of Alpine Tethys with the geological – geophysical record of

spreading and subduction in the Alps, Earth Sci. Rev., 102, 121–158, 2010.

Handy, M. R., Ustaszewski, K., and Kissling, E.: Reconstructing the Alps-Carpathians-Dinarides as key to understanding switches in subduction polarity, slab gaps and surface motion, Int. J. Earth Sci., 104, 1–26, 2015.

Herwegh, M., Berger, A., Baumberger, R., Wehrens, P., and Kissling, E.: Large-scale crustal-block-extrusion during Late Alpine collision, Sci. Rep.-UK, 7, 413, 2017. TS13

Hilgen, F. J., Lourens, L. J., Van Dam, J. A., Beu, A. G., Boyes, A. F., Cooper, R. A., Krijgsman, W., Ogg, J. G., Piller, W. E., and Wilson, D. S.: The Neogene period, in: The geologic time scale, 923–978, 2012. TS14

Homewood, P. and Allen, P. A.: Wave-, Tide-, and Current-Controlled Sandbodies in Miocene Molasse, Western Switzerland, Am. Assoc. Petr. Geol. B., 65, 2534–2545, 1981.

Homewood, P., Allen, P. A. and Williams, G. D.: Dynamics of the Molasse Basin of western Switzerland, Spec. Publs int. Ass. Sediment., 8, 199–217, 1986.

Hurford, A. J.: Cooling and uplift patterns in the Lepontine Alps, south central Switzerland and an age of vertical movement on the Insubric fault line, Contrib. Mineral. Petr., 93, 413–427, 1986.

Isler, A. and Murer, R.: Geologische Karte der Schweiz, Kartenblatt 1149 Wolhusen 1 : 25 000, Bundesamt für Landestopographie swisstopo, in press, 2019. TS15

Jin, J., Aigner, T., Luterbacher, H. P., Bachmann, G. H., and Müller, M.: Sequence stratigraphy and depositional history in the southeastern German Molasse Basin, Mar. Petrol. Geol., 12, 929–940, 1995.

Jordan, T. E.: Thrust loads and foreland basin evolution, Cretaceous, western United States, AAPG Bull., 65, 2506–2520, 1981.

Jordan, T. E. and Flemings, P. B.: Large-scale stratigraphic architecture, eustatic variation, and unsteady tectonism: A theoretical evaluation. J. Geophys. Res.-Sol. Ea., 96, 6681–6699, 1991.

Jost, J., Kempf, O., and Kälin, D.: Stratigraphy and palaeoecology of the Upper Marine Molasse (OMM) of the central Swiss Plateau, Swiss J. Geosci., 109, 149–169, 2016.

Kälin, D. and Kempf, O.: High-resolution stratigraphy from the continental record of the Middle Miocene Northern Alpine Foreland Basin of Switzerland, N. Jb. Geol. Paläont. Abh., 254, 177–235, 2009.

Keller, B.: Fazies und Stratigraphie der Oberen Meeresmolasse (Unteres Miozän) zwischen Napf und Bodensee, PhD, Bern, 302 pp., 1989. TS16

Keller, B.: Wirkung von Wellen und Gezeiten bei der Ablagerung der Oberen Meeresmolasse–Löwendenkmal und Gletschergarten–zwei anschauliche geologische Studienobjekte, Mitteilungen der Naturforschenden Gesellschaft Luzern, 31, 245–271, 1990.

Kempf, O.: Magnetostratigraphy and facies evolution of the Lower Freshwater Molasse (USM) of eastern Switzerland, PhD, Bern, 138 pp., 1998. TS17

Kempf, O. and Matter, A.: Magnetostratigraphy and depositional history of the Upper Freshwater Molasse (OSM) of eastern Switzerland, Eclogae Geol. Helv., 92, 97–103, 1999.

Kempf, O., Bolliger, T., Kälin, D., Engesser, B., and Matter, A.: New magnetostratigraphic calibration of Early to Middle Miocene mammal biozones of the North Alpine foreland basin, Mém. Trav. EPHE Inst. Montpellier, 21, 547–561, 1997.

Kempf, O., Matter, A., Burbank, D. W., and Mange, M.: Depositional and structural evolution of a foreland basin margin in a magnetostratigraphic framework: the eastern Swiss Molasse basin, Int. J. Earth Sci., 88, 253–275, 1999.

Kissling, E. and Schlunegger, F.: Rollback orogeny model for the evolution of the Swiss Alps, Tectonics, 37, 1097–1115, 2018.

Kuhlemann, J.: Post-collisional sediment budget of circum-Alpine basins (Central Europe), Mem. Sci. Geol. Padova, 52, 1–91, 2000.

Kuhlemann, J. and Kempf, O.: Post-Eocene evolution of the North Alpine Foreland Basin and its response to Alpine tectonics, Sediment. Geol., 152, 45–78, 2002.

Kuhlemann, J., Frisch, W., Dunkl, I., Sze ìkely, B., and Spiegel, C.: Miocene shifts of the drainage divide in the Alps and their foreland basin, Z. Geomorphol. N. F., 45, 239–265, 2001a.

Kuhlemann, J., Frisch, W., Dunkl, I., and Székely, B.: Quantifying tectonic versus erosive denudation by the sediment budget: The Miocene core complexes of the Alps, Tectonophysics, 330, 1–23, 2001b.

Kuhlemann, J., Frisch, W., Székely, B., Dunkl, I., and Kázmér, M.: Post-collisional sediment budget history of the Alps: tectonic versus climatic control, Int. J. Earth Sci., 91, 818–837, 2002.

Kühni, A. and Pfiffner, O. A.: The relief of the Swiss Alps and adjacent areas and its relation to lithology and structure: topographic analysis from a 250-m DEM, Geomorphology, 41, 285–307, 2001.

Leclair, S. F. and Bridge, J. S.: Quantitative interpretation of sedimentary structures formed by river dunes, J. Sediment. Res., 71, 713–716, 2001.

Lemcke, K., Engelhardt, W. V., and Füchtbauer, H.: Geologische und sedimentpetrographische Untersuchungen im-Westteil der ungefalteten Molasse des süddeutschen-Alpenvorlandes, Beihefte zum Geologischen Jahrbuch, 11, 1–182, 1953.

Lihou, J. C. and Allen, P. A.: Importance of inherited rift margin structures in the early North Alpine Foreland Basin, Switzerland, Basin Res., 8, 425–442, 1996.

Lippitsch, R., Kissling, E., and Ansorge, J.: Upper mantle structure beneath the Alpine orogen from high-resolution teleseismic tomography, J. Geophys. Res., 108, 2376, 2003. TS18

Lourens, L. J., Hilgen, F. J., Laskar, J., Shackleton, N. J., and Wilson, D.: The Neogene Period. A Geologic Time Scale 2004, Cambridge University Press, 409–440, 2004.

Lu, G., Winkler, W., Rahn, M., von Quadt, A., and Willett, S. D.: Evaluating igneous sources of the Taveyannaz formation in the Central Alps by detrital zircon U–Pb age dating and geochemistry, Swiss J. Geosci., 111, 399–416, 2018.

Malzer, O., Rögl, F., Seifert, P., Wagner, L., Wessely, G., and Brix, F.: Die Molassezone und deren Untergrund. Erdöl und Erdgas in Österreich, 281–322, 1993.

Mancktelow, N.: The Simplon Line: a major displacement zone in the western Lepontine Alps, Eclogae Geol. Helv., 78, 73–96, 1985.

Mancktelow, N. S. and Grasemann, B.: Time-dependent effects of heat advection and topography on cooling histories during erosion, Tectonophysics, 270, 167–195, 1997.

Matter, A.: Sedimentologische Untersuchungen im östlichen Napfgebiet (Entlebuch–Tal der Grossen Fontanne, Kt. Luzern), Eclogae Geol. Helv., 57, 315–429, 1964.

Matter, A., Homewood, P., Caron, C., Rigassi, D., van Stuijvenberg, J., Weidmann, M., and Winkler, W.: Flysch and Molasse of western and central Switzerland, Exc. Guidebook No. 126A, 26th Int. Geol. Congr. Schweiz. Geol. Komm. Wepf and Co. Publ., Basel, 1980.

Mazurek, M. Hurford, A., and Leu, W.: Unravelling the multi-stage burial history of the Swiss Molasse basin: Integration of Apatite fission track, vitrinite reflectance and biomarker isomerisation analysis, Basin Res., 18, 27–50, 2006.

Mein, P.: Résultats du groupe de travail des vertébrés: Biozonation du Néogène méditerranéen à partir des Mammifères, in: Report on Activity of the RCMNS Working groups (1971–1975), edited by: Sénès, J., Bratislava, 78–81, 1975. TS19

Mein, P.: Rapport d'activité du Groupe de Travail Vertébrés Mise à jour de la biostratigraphie du Néogène basée sur les Mammifères, Ann. géol. Pays Héilen., Tome hors série, 3, 1367–1372 (VII International Congress on Mediterranean Neogene, Athens, 1979), 1979. TS20

Mein, P.: Updating of MN zones, in: European Neogene mammal chronology. NATO ASI, Life Sci. 180, edited by: Lindsay, E., Fahlbusch, V., and Mein, P., Plenum Press, New York, 73–90, 1989. TS21

Miall, A. D.: Lithofacies types and vertical profile models in braided river deposits, a summary, in: Fluvial sedimentology, edited by: Miall, A. D., Can. Soc. Petr. Geol. Mem., 5, 597–604, 1978.

Miall, A. D.: Architectural-Element Analysis: A New Method of Facies Analysis Applied to Fluvial Deposits, Earth-Sci. Rev., 22, 261–308, 1985.

Miall, A. D.: The Geology of Fluvial Deposits. Sedimentary Facies, Basin Analysis, and Petroleum Geology, Springer, 582 pp., 1996. TS22

Miller, M. C. and Komar, P. D.: Oscillation Sand Ripples Generated by Laboratory Apparatus, J. Sediment. Res., 50, 173–182, 1980a.

Miller, M. C. and Komar, P. D.: A field investigation of the relationship between oscillation ripple spacinng and the near-bottom water orbital motions, J. Sediment. Res., 50, 183–191, 1980b.

Miller, K. G., Mountain, G. S., the Leg 150 Shipboard Party, and Members of the New Jersey Coastal Plain Drilling Project: Drilling and dating New Jersey Oligocene–Miocene sequences: Ice volume, global sea level, and Exxon records, Science, 271, 92–94, 1996.

Miller, K. G., Mountain, G. S., Browning, J. V., Kominz, M., Sugarman, P. J., Christie-Blick, N., Katz, M. E., and Wright, J. D.: Cenozoic global sea level, sequences, and the New Jersey transect: results from coastal plain and continental slope drilling, Rev. Geophys., 36, 569–601, 1998.

Nichols, P. G.: Sedimentology & Stratigraphy, Blackwell Sci., 355 pp., 1999.

Ortner, H., Fügenschuh, B., Zerlauth, M., Hinsch, R., Friedrich, A., Hofmann, F., and Neumeier, G.: Geometry, sequence and amount of thrusting in the sub-Alpine Molasse of Austria and Bavaria. Fragile Earth: Geological processes from global to local scales and associated hazards: Boulder, Geological Society of America A, 39, 2011. TS23

Pfiffner, O. A.: Evolution of the north Alpine foreland basin in the Central Alps. Special Publication, Int. As. Sed., 8, 219–228, 1986.

Pfiffner, O. A., Schlunegger, F., and Buiter, S. J. H.: The Swiss Alps and their peripheral foreland basin: Stratigraphic response to deep crustal processes, Tectonics, 21, 2002. TS24

Pippèrr, M. and Reichenbacher, B.: Late Early Miocene palaeoenvironmental changes in the North Alpine Foreland Basin, Palaeogeogr. Palaeocl., 468, 485–502, 2017.

Platt, N. H. and Keller, B.: Distal alluvial deposits in a foreland basin setting – the Lower Freshwater Miocene), Switzerland: sedimentology, architecture and palaeosols, Sedimentology, 39, 545–565, 1992.

Python, C.: Geologische Karte der Schweiz, Kartenblatt 1185 Fribourg 1 : 25 000, Bundesamt für Landestopographie swisstopo, 1996.

Reichenbacher, B., Krijgsman, W., Lataster, Y., Pipperr, M., Van Baak, C. G., Chang, L., Kälin, D., Jost, J., Doppler, G., Jung, D., Priet, J., Abdul Aziz, H., Böhme, M., Garnish, J., Kirscher, U., and Bachtadse, V.: A new magnetostratigraphic framework for the Lower Miocene (Burdigalian/Ottnangian, Karpatian) in the North Alpine Foreland Basin, Swiss J. Geosci., 106, 309–334, 2013.

Reichenwallner, S.: Die vulkanische Aktivität in den Westalpen hergeleitet aus detritischem Amphibol und Klinopyroxen im Taveyannaz-Sandstein, unpublished Ms thesis, University of Bern, Bern, 57 pp., 2019.

Reineck, H. E. and Singh, I. B.: Depositional sedimentary environments, Springer, 549 pp., 1980.

Rust, B. R. and Gibling, M. R.: Braidplain evolution in the Pennsylvanian South Bar Formation, Sydney basin, Noca Scotia, Canada, J. Sediment. Petrol., 60, 59–72, 1990.

Salvermoser, S.: Zur Sedimentologie gezeiten-beeinflusster Sande in der Oberen Meeresmolasse und Süssbrackwassermolasse (Ottnangium) von Niederbayern und Oberösterreich, Münchner Geologische Hefte A, 26, 1–179, 1999.

Sant, K. V., Palcu, D., Mandic, O., and Krijgsman, W.: Changing seas in the Early–Middle Miocene of Central Europe: a Mediterranean approach to Paratethyan stratigraphy, Terra Nova, 29, 273–281, 2017.

Schaad, W., Keller, B., and Matter, A.: Die Obere Meeresmolasse (OMM) am Pfänder: Beispiel eines Gilbert-Deltakomplexes, Eclogae Geol. Helv., 85, 145–168, 1992.

Shanmugam, G.: Deep-marine tidal bottom currents and their reworked sands in modern and ancient submarine canyons, Mar. Petroleum Geol., 20, 471–491, 2003.

Schlunegger, F. and Castelltort, S.: Immediate and delayed signal of slab breakoff in Oligo/Miocene Molasse deposits from the European Alps, Sci. Rep.-UK, 6, 31010, 2016. TS25

Schlunegger, F. and Kissling, E.: Slab rollback orogeny in the Alps and evolution of the Swiss Molasse basin, Nat. Commun., 6, 8605, 2015. TS26

Schlunegger, F. and Willett, S.: Spatial and temporal variations in exhumation of the central Swiss Alps and implications for exhumation mechanisms, Geol. Soc. Lond. Spec. Publ., 154, 157–179, 1999.

Schlunegger, F., Burbank, D. W., Matter, A., Engesser, B., and Mödden, C.: Magnetostratigraphic calibration of the Oligocene to Middle Miocene (30–15 Ma) mammal biozones and depositional sequences of the Swiss Molasse Basin, Eclogae Geol. Helv., 89, 753–788, 1996.

Schlunegger, F., Leu, W., and Matter, A.: Sedimentary Sequences, Seismic Facies, Subsidence Analysis, and Evolution of the Burdigalian Upper Marine Molasse Group, Central Switzerland, AAPG Bull., 81, 1185–1207, 1997a.

Schlunegger, F., Jordan, T. E., and Klaper, E. M.: Controls of erosional denudation on foreland basin evolution: The Oligocene central Swiss Molasse Basin as an example, Tectonics, 16, 823–840, 1997b.

Schlunegger, F., Slingerland, R., and Matter, A.: Crustal thickening and crustal extension as controls on the evolution of the drainage network of the central Swiss Alps between 30 Ma and the present: constraints from the stratigraphy of the North Alpine Foreland Basin and the structural evolution of the Alps, Basin Res., 86, 717–750, 1998.

Schlunegger, F., Melzer, J., and Tucker, G.: Climate, exposed source-rock lihtologies, crustal uplift and surface erosion: a theoretical analysis calibrated with data from the Alps/North Alpine Foreland Basin system, Int. J. Earth Sci., 90, 484–499, 2001.

Schlunegger, F., Anspach, O., Bieri, B., Böning, P., Kaufmann, Y., Lahl, K., Lonschinski, M., Mollet, H., Sachse, D., Schubert, C., Stöckli, G., and Zander, I.: Geologische Karte der Schweiz, Kartenblatt 1169 Schüpfheim 1 : 25 000, Bundesamt für Landestopographie swisstopo, 2016.

Schmid, S. M., Pfiffner, O. A., Froitzheim, N., Schönborn, G., and Kissling, E.: Geophysical-geological transect and tectonic evolution of the Swiss-Italian Alps, Tectonics, 15, 1036–1064, 1996.

Schmid, S. M., Fügenschuh, B., Kissling, E., and Schuster, R.: Tectonic map and overall architecture of the Alpine orogen, Eclogae Geol. Helv., 97, 93–117, 2004.

Sinclair, H. D.: Plan-view curvature of foreland basins and its implications for the palaeostrength of the lithosphere underlying the western Alps, Basin Res., 8, 173–182, 1996.

Sinclair, H. D.: Flysch to molasse transition in peripheral foreland basins: The role of the passive margin versus slab breakoff, Geology, 25, 1123–1126, 1997.

Sinclair, H. D. and Allen, P. A.: Vertical versus horizontal motions in the Alpine orogenic wedge: stratigraphic response in the foreland basin, Basin Res., 4, 215–232, 1992.

Sinclair, H. D., Coakley, B. J., Allen, P. A., and Watts, A. B.: Simulation of foreland basin stratigraphy using a diffusion model of mountain belt uplift and erosion: An example from the Central Alps, Switzerland, Tectonics, 10, 599–620, 1991.

Spicher, A.: Tectonic Map of Switzerland, Schweizerische Geologische Kommission, 1980. TS27

Strunck, P. and Matter, A.: Depositional evolution of the western Swiss Molasse, Eclogae Geol. Helv., 95, 197–222, 2002.

Tesauro, M., Kaban, M. K., and Cloething, S. A. P. L.: How rigid is Europe's lithosphere?, Geophys. Res. Lett., 36, 1–6, 2009.

Tesauro, M., Kaban, M. K., and Cloething, S. A. P. L.: Global model for the lithospheric strength and effective elastic thickness, Tectonophysics, 602, 78–86, 2013.

Ustaszewski, K., Schmid, S.M, Fügenschuh, B., Tischler, M., Kissling, E. and Spakman, W.: A map-view restoration of the Alpine-Carpathian-Dinaridic system for the Early Miocene. Swiss Journal of Geosciences, 101 (Suppl. 1), 273–294, 2008.

Waschbusch, P. J. and Royden, L. H.: Spatial and temporal evolution of foredeep basins: lateral strength variations and inelastic yielding in continental lithosphere, Basin Res., 4, 179–196, 1992.

Wanner, J., Gisler, C., Jost, J., Christener, F., and Ninck, T.: Geologische Karte der Schweiz, Kartenblatt 1148 Sumiswald 1 : 25 000, Bundesamt für Landestopographie swisstopo, in press, 2019. TS28

Wehrens, P.: Structural evolution in the Aar Massif (HaslitaI transect): Implications for midcrustal deformation, PhD, Bern, 2015. TS29

Wehrens, P., Baumberger, R., Berger, A., and Herwegh, M.: How is strain localized in a meta-granitoid, mid-crustal basement section? Spatial distribution of deformation in the central Aar massif (Switzerland), J. Struct. Geol., 94, 47–67, 2017.

Willett, S. D.: Late Neogene erosion of the Alps: A climate driver?, Annu. Rev. Earth Pl. Sc., 38, 411–437, 2010.

Yalin, M. S.: Geometrical properties of sand waves, J. Hydr. Div.-ASCE, 90, 105–119, 1964.

Zachos, J., Pagani, M., Sloan, L. Thomas, E., and Billups, K.: Trends, rhythms and aberrations in global climate 65 Ma to present, Science, 292, 686–693, 2001.

Remarks from the language copy-editor

CE1   In keeping with the dominant style of the manuscript, Oxford spellings were not removed.
CE2   Please note the slight edits.

Remarks from the typesetter

TS1   Please confirm initials.
TS2   The composition of all figures except Fig. 3b has been adjusted to our standards. Figs. 1–8 were adjusted for hyphenation and capitalization during copy-editing.
TS3   Please provide a suitable running title.
TS4   Do you mean a or b?
TS5   What does df stand for?
TS6   Please note that units have been changed to exponential format. Please check all instances.
TS7   Could you please provide a new supplement file where also the equations have been numbered as S1, S2, S3, etc.? Thank you very much in advance.
TS8   Please note that the funding information has been added to this paper. Please check if it is correct. Please also double-check your acknowledgements to see whether repeated information can be removed or changed accordingly. Thanks.
TS9   Please note that the funding information has been added to this paper. Please check if it is correct. Please also double-check your acknowledgements to see whether repeated information can be removed or changed accordingly. Thanks.
TS10   Please provide publisher and place of publication.
TS11   Not mentioned in the text.
TS12   Please provide page range or DOI and article number.
TS13   Please provide page range or DOI and article number.
TS14   Please provide publisher and place of publication. Furthermore, this reference is not mentioned in the text.
TS15   If possible, please update.
TS16   If possible, please add university.
TS17   If possible, please add university.
TS18   Please provide DOI.
TS19   Please provide publisher. Furthermore, this reference is not mentioned in the text.
TS20   Not mentioned in the text.
TS21   Not mentioned in the text.
TS22   Please provide place of publication.
TS23   Please provide page range or DOI and article number.
TS24   Please provide page range or DOI and article number.
TS25   Please provide DOI.
TS26   Please provide page range or DOI and article number.
TS27   Please provide place of publication.
TS28   If possible, please update.
TS29   If possible, please provide university.